Integrating artificial intelligence-based epitope prediction in a SARS-CoV-2 antibody discovery pipeline: caution is warranted

Delphine Diana Acar, Wojciech Witkowski, Magdalena Wejda, Ruifang Wei, Tim Desmet, Bert Schepens, Sieglinde de Cae, Koen Sedeyn, Hannah Eeckhaut, Daria Fijalkowska, et al.

Integrating artificial intelligence-based epitope prediction in a SARS-CoV-2 antibody discovery pipeline: caution is warranted

Delphine Diana Acar,[a,k] Wojciech Witkowski,[a,k] Magdalena Wejda,[a] Ruifang Wei,[a] Tim Desmet,[b] Bert Schepens,[c,d] Sieglinde De Cae,[c,d] Koen Sedeyn,[c,d] Hannah Eeckhaut,[c,d] Daria Fijalkowska,[c,d] Kenny Roose,[c,d] Sandrine Vanmarcke,[c,d] Anne Poupon,[e] Dirk Jochmans,[f] Xin Zhang,[f] Rana Abdelnabi,[f] Caroline S. Foo,[f] Birgit Weynand,[g] Dirk Reiter,[h] Nico Callewaert,[c,d] Han Remaut,[h,i] Johan Neyts,[f] Xavier Saelens,[c,d] Sarah Gerlo,[a,j,l] and Linos Vandekerckhove[a,l,*]

[a]HIV Cure Research Center, Department of Internal Medicine and Pediatrics, Ghent University Hospital, Ghent University, Ghent 9000, Belgium
[b]Department of Basic and Applied Medical Sciences, Ghent University, Ghent 9000, Belgium
[c]VIB-UGent Center for Medical Biotechnology, VIB, Ghent 9052, Belgium
[d]Department of Biochemistry and Microbiology, Ghent University, Ghent 9052, Belgium
[e]MAbSilico, Tours 37000, France
[f]Laboratory of Virology and Chemotherapy, Department of Microbiology, Immunology and Transplantation, Rega Institute for Medical Research, KU Leuven, Leuven 3000, Belgium
[g]Department of Imaging and Pathology, Translational Cell and Tissue Research, KU Leuven, Leuven 3000, Belgium
[h]Department of Bioengineering Sciences, Vrije Universiteit Brussel, Brussels 1050, Belgium
[i]VIB-VUB Center for Structural Biology, VIB, Brussels 1050, Belgium
[j]Department of Biomolecular Medicine, Ghent University, Ghent 9000, Belgium

eBioMedicine
2024;100: 104960
Published Online xxx
https://doi.org/10.1016/j.ebiom.2023.104960

Summary

Background SARS-CoV-2-neutralizing antibodies (nABs) showed great promise in the early phases of the COVID-19 pandemic. The emergence of resistant strains, however, quickly rendered the majority of clinically approved nABs ineffective. This underscored the imperative to develop nAB cocktails targeting non-overlapping epitopes.

Methods Undertaking a nAB discovery program, we employed a classical workflow, while integrating artificial intelligence (AI)-based prediction to select non-competing nABs very early in the pipeline. We identified and *in vivo* validated (in female Syrian hamsters) two highly potent nABs.

Findings Despite the promising results, in depth cryo-EM structural analysis demonstrated that the AI-based prediction employed with the intention to ensure non-overlapping epitopes was inaccurate. The two nABs in fact bound to the same receptor-binding epitope in a remarkably similar manner.

Interpretation Our findings indicate that, even in the Alphafold era, AI-based predictions of paratope-epitope interactions are rough and experimental validation of epitopes remains an essential cornerstone of a successful nAB lead selection.

Funding Full list of funders is provided at the end of the manuscript.

Keywords: SARS-CoV-2; Neutralizing antibody; *In silico* prediction; Epitope mapping; Covid-19

Introduction

Monoclonal antibody cloning from single B cells is becoming accessible to a growing number of academic and industrial laboratories. The unprecedented speed of SARS-CoV-2 neutralizing antibody (nAB) development illustrates this accessibility. Within a few months from the start of the COVID-19 pandemic multiple clinical trials were initiated to evaluate the efficacy of nAbs leading to their market authorization by respective agencies worldwide. Currently, REGN-COV2,[1] LY-CoV555, either alone or in combination with LY-CoV016,[2–4] VIR 7831,[5] and other anti-SARS-CoV-2

*Corresponding author.
E-mail address: linos.vandekerckhove@ugent.be (L. Vandekerckhove).
[k]Both authors contributed equally.
[l]Both share senior authorship.

Research in context

Evidence before this study

In silico modelling of antibody-epitope interactions, if accurate, can save time and resources allowing for streamlined development of therapeutics. We queried PubMed for publications on epitope prediction published between 2013 and 2023 using search terms such as "antibody-epitope prediction", "*in silico* epitope mapping", "sequence based antibody prediction" and "AI antibody prediction". Numerous studies describe computational methods for sequence-based antibody modelling, however true experimental validation of such models is scarce.

Added value of this study

Within the context of this study, AI-assisted epitope prediction was used as the sole method for lead selection while BLI, mutation screening and cryo-EM analyses were performed subsequently.

Implications of all the available evidence

Results of this study indicate that performance of AI-based methods for *de novo* prediction lacks accuracy and still requires experimental input.

Spike (S) antibodies are emergency-approved for therapeutic or preventive use (reviewed in Kumar, Chandele[6]). SARS-CoV-2 has, however, been shown to rapidly evolve,[7] occasionally accumulating multiple mutations even within one host.[8,9] The resulting continuous emergence of COVID-19 variants of concern (VOC) with Omicron as notable example has already deemed most of these nABs ineffective.[10] Since several medical conditions result in impaired immune responses to both SARS-CoV-2 infection and vaccination, effective nAbs must be available for clinical interventions. In this light, rapid epitope mapping of potential nAb candidates is essential in discovery pipelines. Several experimental techniques at various levels of complexity such as biolayer interferometry, yeast display-based deep mutational scanning, or cryo-EM allow to obtain that information. In addition, recently artificial-intelligence (AI)-based methods have been used to predict epitopes for Abs with unknown 3D structures.[11–14]

Here, we describe the isolation and characterization of two potently neutralizing antibodies against the SARS-CoV-2 receptor binding domain (RBD) from convalescent patient-derived B cells. Combining information from pseudovirus neutralization assays with *in silico* epitope prediction via MabTope,[15] we selected for further testing two nABs with neutralization potencies in the picomolar range and predicted not to compete with each other. *In vivo* experiments in a hamster model of SARS-CoV-2 infection demonstrated efficacy of the selected nABs cocktail to be lower than anticipated. Although unexpected based on the AI epitope predictions (except for K417, predicted as part of the UZGENT_A3 epitope), our antibody cocktail lost efficacy against selected VOCs (Beta and Omicron). Ultimately, determination of the SARS-CoV-2-RBD-Antibody complex structures via cryo-EM revealed that the two antibodies interact with the RBD in a very similar manner with largely overlapping epitopes, explaining their loss of performance in neutralizing selected SARS-CoV-2 variants.

Methods

Ethics statement

Human subjects

A total of 151 convalescent COVID-19 patients with disease severities ranging from mild (CoSer cohort, 72 individuals) to severe (CoVim cohort, 79 individuals) for whom diagnosis was either confirmed by PCR and/or ELISA (Supplementary Table S2) were enrolled in this study and thus subjected to a single blood draw. Patient sampling was approved by the Ghent University Hospital's Ethical Committee (applications BC-07492 and BC-08071) and all participants provided a written informed consent.

Animals

Wild-type Syrian Golden hamsters (*Mesocricetus auratus*) were purchased from Janvier Laboratories and were housed per two in ventilated isolator cages (IsoCage N Biocontainment System, Tecniplast) with *ad libitum* access to food and water and cage enrichment (wood block). In the described experiment, only female hamsters of 6–8 weeks old were used and animals were acclimated for 4 days prior to study start. Housing conditions and experimental procedures were approved by the ethics committee of animal experimentation of KU Leuven (license P065-2020).

Cell lines

HEK293-T cells (ATCC CRL-3216) utilized for pseudotyped HIV and small scale antibody production were cultured in Dulbecco's Modified Eagle's Medium (DMEM, Gibco) with 10% fetal bovine serum (FBS, HyClone), 1% penicillin (Gibco), 1% streptomycin (Gibco) and 1% L-glutamine (Gibco) at 37 °C with 5% CO_2 in a humidified incubator. TZM-bl cells contributed by Dr. John C. Kappes and Dr. Xiaoyun Wu were obtained through the NIH HIV Reagent Program, Division of AIDS, NIAID, NIH (ARP-8129). They are derived from a HeLa cell line, contain a β-galactosidase gene driven by a Tat-responsive human immunodeficiency virus (HIV) LTR promoter, and were cultured in

DMEM (Gibco) supplemented with 10% FBS (HyClone), 1% L-glutamine (Gibco), 1% penicillin and 1% streptomycin (Gibco), under 5% CO_2 atmosphere in a humidified incubator set to 37 °C. HEK293-T cells (ATCC CRL-3216) used for pseudotyped VSV production and Vero E6 cells (ATCC CRL-1586) employed in VSV pseudotype neutralization experiments were cultured at 37 °C in the presence of 5% CO_2 in DMEM (Gibco) supplemented with 10% FBS (TICO), 1% penicillin (Sigma-Aldrich), 1% streptomycin (Sigma-Aldrich), 2 mM L-glutamine, 1% non-essential amino acids (Sigma-Aldrich) and 1 mM sodium pyruvate (Sigma-Aldrich). HEK293-S cells[16] were cultured in FreeStyle293 expression media (Life Technologies) at 37 °C with 8% CO_2 while shaking at 130 rpm. Vero E6 cells (ATCC CRL-1586) used for titration of the SARS-CoV-2 virus stocks and in SARS-CoV-2 plaque reduction neutralization tests were cultured in Minimum Essential Medium (MEM, Gibco) supplemented with 10% FBS, 1% L-glutamine (Gibco) and 1% bicarbonate (Gibco) at 37 °C with 5% CO_2. End-point titrations were performed with medium containing 2% FBS instead of 10%. ExpiCHO-S cells (ThermoFisher Scientific) were cultured according to the manufacturer's protocol. Briefly, cells were grown in vented polycarbonate flat-bottom erlenmeyers (Corning) in ExpiCHO expression medium (ThermoFisher Scientific) at 37 °C, 8% CO_2 and 125 rpm in a shaking incubator (25 mm throw). Cell lines were validated by the suppliers and are routinely tested for mycoplasma.

Virus strains

The SARS-CoV-2 strain BetaCov/Belgium/GHB-03021/2020 (EPI ISL 109 407976|2020-02-03), was recovered from a nasopharyngeal swab taken from an RT-qPCR confirmed asymptomatic patient who returned from Wuhan, China in the beginning of February 2020. A close relation with the prototypic Wuhan-Hu-1 2019-nCoV (GenBank accession 112 number MN908947.3) strain was confirmed by phylogenetic analysis. Infectious virus was isolated by serial passaging on HuH7 and Vero E6 cells[17]; passage 6 virus was used for the hamster study described below.

Passage 2 SARS-CoV-2 virus stocks belonging to lineages B.1.1.7., B.1.351, B.1.617.2 and B.1.1.529 virus stocks were grown on Vero E6 cells. The SARS-CoV-2 B.1.1.7 (hCoV-19/Belgium/rega-12211513/2020; EPI_ISL_791333, 2020-12-21), B.1.351 (hCoV-19/Belgium/rega-1920/2021; EPI_ISL_896474, 2021-01-11), B.1.617.2 (hCoV-19/Belgium/rega-7214/2021; EPI_ISL_2425097; 2021-04-20) and B.1.1.529 (hCoV-19/Belgium/rega-20174/2021, EPI_ISL_6,794,907) isolates were each retrieved from nasopharyngeal swabs taken from travellers returning to Belgium in 2020 and 2021 and have recently been described.[18–20]

The titer of the virus stocks was determined by end-point dilution on Vero E6 cells by the Reed and Muench method.[21] Live virus-related work was conducted in the high-containment A3 and BSL3+ facilities of the KU Leuven Rega Institute (3CAPS) under licenses AMV 30112018 SBB 219 2018 0892 and AMV 23102017 SBB 219 20170589 according to institutional guidelines.

Method details

Identification and production of antibodies

Production of recombinant His- and Fc-tagged SARS-CoV-2 spike RBD-SD1 protein. To obtain recombinant His- and Fc-tagged SARS-CoV-2 Spike RBD-SD1 protein, suspension-adapted and serum-free HEK293-S cells were transiently transfected with a pαH expression vector containing the coding sequence of SARS-CoV-2 RBD-SD1 (residues 319–591) upstream of a C-terminal HRV3C protease cleavage site, a monomeric Fc tag and an 8 × His tag (kind gift from Jason McLellan).[22] Briefly, cells were seeded in FreeStyle 293 expression medium (Gibco) at a cell density of 3.0×10^6 cells/mL. Cells were transfected by adding 4.5 μg expression vector per mL cells for 5 min, followed by the addition of 9 μg polyethylenimine (Polysciences) per mL cells. After 5 h of incubation at 37 °C, an equal volume of EX-CELL 293 medium (Sigma-Aldrich) was added. After 3 days, 5 g/L D-glucose was added to extend the cell viability and supernatant was harvested 4 days post-transfection. The supernatant was cleared by centrifugation (15 min at 250×g) and filtration. The protein was then purified from the supernatant by immobilized metal ion affinity chromatography (HisTrap HP column, Cytiva), buffer exchanged to PBS by using a HiPrep 26/10 desalting column (Cytiva), and finally filtered over a low protein binding 0.2 μm filter.

Isolation of anti-SARS-CoV-2 antibody-producing B cells. Peripheral blood mononuclear cells were isolated from blood samples of the convalescent COVID-19 patient samples through Ficoll density gradient centrifugation and B cells were extracted by magnetic-activated cell sorting using the B Cell Isolation Kit II human (Miltenyi Biotec) according to the manufacturer's instructions. The enriched B cells were first incubated with the Viability 405/452 Fixable Dye (Miltenyi Biotec) for 15 min at room temperature, subsequently for 30 min on ice with in-house produced recombinant His- and Fc-tagged SARS-CoV-2 Spike RBD-SD1 protein and, and finally with anti-CD3-BV421 (BD Biosciences), anti-CD14-BV421 (BD Biosciences), anti-CD16-BV421 (BD Biosciences), anti-CD27-PE-Cy7 (BD Biosciences), anti-CD19-FITC (Miltenyi Biotec), anti-His-PE (Miltenyi Biotec) and anti-His-APC (Miltenyi Biotec) for 30 min on ice. AutoMACS Rinsing Solution (Miltenyi Biotec) supplemented with 0.5% BSA (Miltenyi Biotec) was used to prepare the RBD and antibody solutions and to wash the cells after the different staining steps. Single cells were sorted directly into lysis buffer that consisted of 0.5 × PBS, 10 mM DTT and 2 U/μl RNasin Plus

(Promega) with a BD FACSAria™ Fusion (BD Biosciences), immediately frozen on dry ice and stored at –80 °C.

RT-PCR, cloning and sequencing. Synthesis of cDNA was performed using Superscript III (Invitrogen) and a reverse primer mix containing equimolar amounts of primers 3′CγCH1, 3′Cκ543 and 3′Cλ (see table below[23]). The reverse transcription mixes furthermore contained 0.06% Igepal (Sigma-Aldrich) to additionally stimulate cell lysis. Following cDNA synthesis, genes that encode the immunoglobulin heavy and light chain variable domains were amplified using the Q5 High-Fidelity 2X Master Mix (New England BioLabs) and different primer sets (see table below[23]). Amplicons from the first PCR reaction subsequently served as templates for a second PCR reaction, during which primers (see table below[24]) were employed that incorporate sequences homologous to defined regions of human immunoglobulin expression vectors that already contain the immunoglobulin heavy and light constant domains, i.e., AbVec2.0-IGHG1 (Addgene plasmid #80795), AbVec1.1-IGKC (Addgene plasmid #80796) and AbVec1.1-IGLC2-XhoI (Addgene plasmid #99575).[23] PCR products from the second reaction were purified using the NucleoSpin 96 PCR Clean-up kit (Macherey-Nagel) following the manufacturer's instructions and subsequently used for homology-based cloning with the HiFi DNA Assembly Master Mix (New England BioLabs) to insert them into the expression vectors. Preparation of pure plasmid DNA from small- and large-scale bacterial cultures was respectively performed with the NucleoSpin 96 Plasmid kit (Macherey-Nagel) and the NucleoBond Xtra Midi kit (Macherey-Nagel). The antibody variable region nucleic acid sequences that were cloned into the expression vectors were determined by Sanger sequencing with the FWD-IGHLK primer (see table below) and computational analyses of the antibody sequences were performed using the publicly available scripts and data on GitHub (https://github.com/stratust/igpipeline) as described by Robbiani, Gaebler.[25]

Primers (5′ → 3′) used for reverse transcription (RT), PCR amplification of the antibody sequences and Sanger sequencing:

Small scale antibody production. For transient monoclonal antibody expression, HEK293-T cells were transfected with a roughly equal amount of plasmid DNA encoding the light chain and the heavy chain using the CalPhos™ Mammalian Transfection Kit (Takara) according to the manufacturer's protocol. Briefly, HEK293-T cells were seeded at a density of 10,000 cells per well in 96-well plates and incubated at 37 °C for 24 h in a humidified 5% CO_2 incubator. Calcium phosphate-DNA precipitates were prepared by first combining 0.5 µl of 2 M CaCl2 with 50–150 ng of total plasmid DNA mix in a final volume of 4 µl, followed by adding an equal volume of 2 × HEPES-buffered saline. The mixtures were vortexed vigorously for 5 min and incubated for another 5 min before they were added to the cells. Cells were washed and refreshed with Opti-MEM™ (ThermoFisher Scientific) one day after transfection. The supernatants were collected three days afterwards (4 days post-transfection) and stored at –20 °C until further analysis.

Large scale antibody production and purification. Antibodies were expressed in ExpiCHO-S™ cells (ThermoFisher Scientific), according to the manufacturer's protocol. Briefly, a 200 mL culture of 6 × 106 cells per mL, grown at 37 °C and 8% CO_2, was transfected with a 2:1 combination of plasmid DNA encoding the light chain (107 µg DNA) and the heavy chain (53 µg DNA) using ExpiFectamine™ CHO reagent. One day after transfection, 1200 µl ExpiCHO™ enhancer and 32 mL ExpiCHO™ feed was added to the cells, and cultures were further incubated at 32 °C and 5% CO_2. Cells were fed a second time on day 5 after transfection. Productions were collected as soon as the cell viability dropped below 75% by pelleting the cells and filtering the supernatant through a 0.22 µm bottle top filter. Cleared supernatants were stored at 4 °C until further processing.

For purification of the antibodies, supernatants were loaded on a 5 mL MAbSelect SuRe column (GE Healthcare). Unbound proteins were washed away with McIlvaine buffer pH 7.2, and bound proteins were eluted using McIlvaine buffer pH 3. Immediately after elution, protein-containing fractions were neutralized using a saturated (0.4 M) Na3PO4 buffer. Next, these

Primer name	Polarity	Purpose	Primer sequence
5′L-VH1	Sense	PCR 1	ACAGGTGCCCACTCCCAGGTGCAG
5′L-VH3	Sense	PCR 1	AAGGTGTCCAGTGTGARGTGCAG
5′L-VH4/6	Sense	PCR 1	CCCAGATGGGTCCTGTCCCAGGTGCAG
5′L-VH5	Sense	PCR 1	CAAGGAGTCTGTTCCGAGGTGCAG
5′LVκ1/2	Sense	PCR 1	ATGAGGSTCCCYGCTCAGCTGCTGG
5′LVκ3	Sense	PCR 1	CTCTTCCTCCTGCTACTCTGGCTCCCAG
5′LVκ4	Sense	PCR 1	ATTTCTCTGTTGCTCTGGATCTCTG

(continues on next page)

Primer name	Polarity	Purpose	Primer sequence
(Continued from previous page)			
5′LVλ1	Sense	PCR 1	GGTCCTGGGCCCAGTCTGTGCTG
5′LVλ2	Sense	PCR 1	GGTCCTGGGCCCAGTCTGCCCTG
5′LVλ3	Sense	PCR 1	GCTCTGTGACCTCCTATGAGCTG
5′LVλ4/5	Sense	PCR 1	GGTCTCTCTCSCAGCYTGTGCTG
5′LVλ6	Sense	PCR 1	GTTCTTGGGCCAATTTTATGCTG
5′LVλ7	Sense	PCR 1	GGTCCAATTCYCAGGCTGTGGTG
5′LVλ8	Sense	PCR 1	GAGTGGATTCTCAGACTGTGGTG
VH 1 SLIC	Sense	PCR 2	CTAGTAGCAACTGCAACCGGTGTACATTCCCAGGTGCAGCTGGTGCAG
VH 1/5 SLIC	Sense	PCR 2	CTAGTAGCAACTGCAACCGGTGTACATTCCGAGGTGCAGCTGGTGCAG
VH 1-18 SLIC	Sense	PCR 2	CTAGTAGCAACTGCAACCGGTGTACATTCCCAGGTTCAGCTGGTGCAG
VH 1-24 SLIC	Sense	PCR 2	CTAGTAGCAACTGCAACCGGTGTACATTCCCAGGTCCAGCTGGTACAG
VH 3 SLIC	Sense	PCR 2	CTAGTAGCAACTGCAACCGGTGTACATTCTGAGGTGCAGCTGGTGGAG
VH 3-23 SLIC	Sense	PCR 2	CTAGTAGCAACTGCAACCGGTGTACATTCTGAGGTGCAGCTGTTGGAG
VH 3-33 SLIC	Sense	PCR 2	CTAGTAGCAACTGCAACCGGTGTACATTCTCAGGTGCAGCTGGTGGAG
VH 3-9 SLIC	Sense	PCR 2	CTAGTAGCAACTGCAACCGGTGTACATTCTGAAGTGCAGCTGGTGGAG
VH 4 SLIC	Sense	PCR 2	CTAGTAGCAACTGCAACCGGTGTACATTCCCAGGTGCAGCTGCAGGAG
VH 4-34 SLIC	Sense	PCR 2	CTAGTAGCAACTGCAACCGGTGTACATTCCCAGGTGCAGCTACAGCAGTG
VH 4-39 SLIC	Sense	PCR 2	CTAGTAGCAACTGCAACCGGTGTACATTCCCAGCTGCAGCTGCAGGAG
VH 6-1 SLIC	Sense	PCR 2	CTAGTAGCAACTGCAACCGGTGTACATTCCCAGGTACAGCTGCAGCAG
VK 1-5 SLIC	Sense	PCR 2	GTAGCAACTGCAACCGGTGTACATTCTGACATCCAGATGACCCAGTC
VK 1-9 SLIC	Sense	PCR 2	GTAGCAACTGCAACCGGTGTACATTCAGACATCCAGTTGACCCAGTCT
VK 1D-43 SLIC	Sense	PCR 2	GTAGCAACTGCAACCGGTGTACATTGTGCCATCCGGATGACCCAGTC
VK 2-24 SLIC	Sense	PCR 2	GTAGCAACTGCAACCGGTGTACATGGGGATATTGTGATGACCCAGAC
VK 2-28 SLIC	Sense	PCR 2	GTAGCAACTGCAACCGGTGTACATGGGGATATTGTGATGACTCAGTC
VK 2-30 SLIC	Sense	PCR 2	GTAGCAACTGCAACCGGTGTACATGGGGATGTTGTGATGACTCAGTC
VK 3-11 SLIC	Sense	PCR 2	GTAGCAACTGCAACCGGTGTACATTCAGAAATTGTGTTGACACAGTC
VK 3-15 SLIC	Sense	PCR 2	GTAGCAACTGCAACCGGTGTACATTCAGAAATAGTGATGACGCAGTC
VK 3-20 SLIC	Sense	PCR 2	GTAGCAACTGCAACCGGTGTACATTCAGAAATTGTGTTGACGCAGTCT
VK 4-1 SLIC	Sense	PCR 2	GTAGCAACTGCAACCGGTGTACATTCGGACATCGTGATGACCCAGTC
VL 1 SLIC	Sense	PCR 2	CTAGTAGCAACTGCAACCGGTTCCTGGGCCCAGTCTGTGCTGACKCAG
VL 2 SLIC	Sense	PCR 2	CTAGTAGCAACTGCAACCGGTTCCTGGGCCCAGTCTGCCCTGACTCAG
VL 3 SLIC	Sense	PCR 2	CTAGTAGCAACTGCAACCGGTTCTGTGACCTCCTATGAGCTGACWCAG
VL 4/5 SLIC	Sense	PCR 2	CTAGTAGCAACTGCAACCGGTTCTCTCTCSCAGCYTGTGCTGACTCA
VL 6 SLIC	Sense	PCR 2	CTAGTAGCAACTGCAACCGGTTCTTGGGCCAATTTTATGCTGACTCAG
VL 7/8 SLIC	Sense	PCR 2	CTAGTAGCAACTGCAACCGGTTCCAATTCYCAGRCTGTGGTGACYCAG
FWD-IGHLK	Sense	Sequencing	CACCCCCTTGGCTTCGTTAG
3′CγCH1	Antisense	RT and PCR 1	GGAAGGTGTGCACGCCGCTGGTC
3′Cκ543	Antisense	RT and PCR 1	GTTTCTCGTAGTCTGCTTTGCTCA
3′Cλ	Antisense	RT and PCR 1	CACCAGTGTGGCCTTGTTGGCTTG
JH 1/2/4/5 SLIC	Antisense	PCR 2	CGCTTGGGCCCTTGGTCGACGCTGAGGAGACGGTGACCAG
JH 3 SLIC	Antisense	PCR 2	CGCTTGGGCCCTTGGTCGACGCTGAAGAGACGGTGACCATTG
JH 6 SLIC	Antisense	PCR 2	CGCTTGGGCCCTTGGTCGACGCTGAGGAGACGGTGACCGTG
JK 1/4 SLIC	Antisense	PCR 2	GAAGACAGATGGTGCAGCCACCGTACGTTTGATYTCCACCTTGGTC
JK 2 SLIC	Antisense	PCR 2	GAAGACAGATGGTGCAGCCACCGTACGTTTGATCTCCAGCTTGGTC
JK 3 SLIC	Antisense	PCR 2	GAAGACAGATGGTGCAGCCACCGTACGTTTGATATCCACTTTGGTC
JK 5 SLIC	Antisense	PCR 2	GAAGACAGATGGTGCAGCCACCGTACGTTTAATCTCCAGTCGTGTC
CL SLIC	Antisense	PCR 2	GGCTTGAAGCTCCTCACTCGAGGGYGGGAACAGAGTG

fractions were pooled, and loaded on a HiPrep Desalting column for buffer exchange to storage buffer (DPBS pH 7.4). Purified antibodies were filter-sterilized using a 0.22 μm filter, batched out and stored at –80 °C until use.

Generation of N59Q mutants of UZGENT_A3 and UZ_GENT_G5. Plasmids encoding heavy chains of UZGENT_A3 and UZ_GENT_G5 were subjected to PCR reactions with primers containing mismatches resulting in AAC to CAG codon change.

Primer name	Polarity	Primer sequence
UZGENT_A3 HC-N59Q	Sense	GATCAACCCTAACAGTGGCGGAACACAGTACACACAGAAGTTTAAG
UZGENT_A3 HC-N59Q	Antisense	CTTAAACTTCTGTGTGTACTGTGTTCCGCCACTGTTAGGGTTGATC
UZGENT_G5 HC-N59Q	Sense	CTATCAGTGGTGCCACACAGTATACACAGAAGTTTCAGGG
UZGENT_G5 HC-N59Q	Antisense	CCCTGAAACTTCTGTGTATACTGTGTGGCACCACTGATAG

Following thermal cycling with PfuTurbo DNA polymerase, Dpn1 endonuclease was used to digest the template DNA. PCR products were then transformed into competent DH5a cells (New England Biolabs). Preparation of pure plasmid DNA was performed with the NucleoSpin 96 Plasmid kit (Machery-Nagel). Presence of desired mutations was confirmed by Sanger sequencing. UZGENT_A3, UZ_GENT_G5 and their N59Q mutants were then produced in HEK293Ts as described above and purified on Protein G spin columns according to the manufacturer guidelines (Thermo Scientific). Eluates were subjected to desalting and concentration using Amicon Ultra columns with 50 kDa filters (Merck Millipore).

Anti-SARS-CoV-2 S1 ELISA

The Anti-SARS-CoV-2 ELISA (IgG) from EUROIMMUN was used to evaluate antibodies binding to SARS-CoV-2 S1. The assay was performed according to the manufacturer's instructions using a 1:20 dilution of crude supernatants from transformed HEK293-T cells. After photometric measurement of the colour intensity made at a wavelength of 450 nm and a reference wavelength of 620 nm, the ratio of the extinction of samples over the extinction of the included calibrator was calculated. Samples were considered positive if the value of the obtained ratio exceeded 0.8.

HIV-based pseudovirus neutralization assay

Pseudovirus production. Pseudovirions were generated by transiently transfecting HEK293-T cells with HIV-1 SG3ΔEnv non-infectious molecular clone and a lentiviral vector expressing the codon optimized SARS-CoV-2 spike using jetOPTIMUS DNA transfection reagent (Polyplus-transfection). The HIV-1 SG3ΔEnv Non-infectious Molecular Clone, ARP-11051, was obtained through the NIH HIV Reagent Program, Division of AIDS, NIAID, NIH and contributed by Drs. John C. Kappes and Xiaoyun Wu. pBOB-CAG-SARS-CoV2-spike-HA was a gift from Gerald Pao (Addgene plasmid #141347[26]). To allow pseudotyping, the packaging signal was deleted from pBOB-CAG-SARS-CoV2-spike-HA by digestion with NdeI restriction enzyme (New England BioLabs). Sixteen hours after transfection, the medium was changed, and 48 h after transfection supernatant containing virus was collected and concentrated by centrifugation in Amicon Ultra-15 MWCO 100 kDa centrifugal filters. Concentrated viral supernatant containing spike-pseudotyped HIV-1 virions were frozen at –80 °C for long-term storage or used immediately in the neutralization assay.

Neutralization assay. For the initial neutralization experiments, 30 µl of pseudotyped HIV-1 was mixed with 20 µl of crude supernatants from transformed HEK293T cells that contain the produced antibodies and incubated at 37 °C for 30 min. Subsequently, 50 µl of TZM-bl/ACE2 cells[27] were added, and the mixture was centrifuged for 30 min at 2300 rpm 32 °C. Polybrene (Merck Millipore) was added at the final concentration of 5 µg/mL to facilitate the infection. After an incubation period of 18 h in a 5% CO_2 incubator at 37 °C, the cell medium was refreshed, and the colorimetric readout was performed using the β-Galactosidase Assay Reagent (Thermo Scientific) following manufacturer's instructions after 48 h. Absorbance was measured using Multiskan FC microplate spectrophotometer with 405 nm filter (Thermo Scientific). Neutralization percentages were then calculated as follows:

$$1-\frac{\left(\text{extinction}_{\text{sample}}-\text{extinction}_{\text{no virus,no antibody}}\right)}{\text{extinction}_{\text{virus only}}}*100$$

Samples were considered positive if the obtained neutralization percentage equaled or exceeded 10%.

VSV-based pseudovirus neutralization assay

Pseudovirus production. To generate replication-deficient VSV pseudotyped viruses, HEK293-T cells, that were transfected with an expression vector encoding the spike protein of SARS-CoV-2 S or the mutants thereof were inoculated with a replication deficient VSV vector containing eGFP and firefly luciferase expression cassettes.[28,29] After a 1 h incubation at 37 °C, the inoculum was removed, cells were washed with PBS and incubated in media supplemented with an anti-VSV G mAb (ATCC) for 16 h. Pseudotyped particles were then harvested and clarified by centrifugation.[22]

Neutralization assay. For more robust and sensitive readouts, VSV pseudotype neutralization experiments were performed, whereby, pseudoviruses were incubated for 30 min at room temperature with different

concentrations of the purified antibodies. The incubated pseudoviruses were subsequently added to confluent monolayers of Vero E6 cells. Sixteen hours later, the cells were lysed using passive lysis buffer (Promega). The transduction efficiency was quantified by measuring the GFP fluorescence in the prepared cell lysates using a Tecan infinite 200 pro plate reader. The GFP fluorescence was normalized using the GFP fluorescence of non-infected cells and of infected cells treated with PBS that were included in each dilution series. The IC50 was calculated by nonlinear regression curve fitting, log(inhibitor) vs. normalized response with variable slope.

SARS-CoV-2 plaque reduction neutralization test

Dose-dependent neutralization of distinct antibodies was assessed by mixing different concentrations of the purified antibodies with 100 PFU SARS-CoV-2 in DMEM supplemented with 2% FBS and incubating the mixture at 37 °C for 1 h. Antibody-virus complexes were then added to Vero E6 cell monolayers in 12-well plates and incubated at 37 °C for 1 h. Subsequently, the inoculum mixture was replaced with 1.6% (w/v) methylcellulose in DMEM supplemented with 2% FBS. After 3 or 4 days incubation at 37 °C, the overlays were removed, the cells were fixed with 3.7% PFA, stained with 1% crystal violet, and plaques were counted.

Bio-layer interferometry

All assays were performed with anti-human IgG Fc capture sensors (ForteBio) on an Octet RED96 system (ForteBio) at 30 °C with shaking at 1000 rpm. Data were recorded with the Octet Data Acquisition software version 10.0 (ForteBio).

Kinetics and affinity analysis. After immersion of the biosensors in kinetics buffer that consisted of PBS + 0.1% BSA + 0.02% Tween 20 (baseline 1; 60 s), antibodies (1 μg/mL) were captured (loading; 300 s). After recording a second baseline signal (baseline 2: 60 s), the sensors were immersed into wells containing serial dilutions of purified His-tagged SARS CoV-2 RBD (association; 300 s), a kind gift from BioMARIC NV, followed by immersion in kinetics buffer (dissociation; 700 s). The experiment was performed in triplicate and data were analysed as described below for each of the replicates to obtain three independent values for the affinity constant (K_D) and association and dissociation rates (k_{on} and k_{off}, respectively).

Epitope binning. Binning assays were performed with a "classical sandwich" approach: biosensors were immersed consecutively in (1) kinetics buffer (baseline 1; 30 s), (2) antibody 1 solution (loading; 600 s; 1 μg/mL), (3) kinetics buffer (baseline 2; 30 s), (4) human IgG isotype control solution (quenching; 300 s; 100 μg/mL), (5) kinetics buffer (baseline 3; 30 s), (6) purified His-tagged SARS CoV-2 RBD (association; 300 s; 100 nM), (7) kinetics buffer (baseline 4; 30 s), (8) antibody 2 solution (association; 300 s; 1 μg/mL).

In silico epitope prediction

Epitope mapping using artificial intelligence-based methods were not performed in-house but outsourced to MAbSilico, a company that applies a range of self-developed algorithms to establish computational epitope binning and mapping as described by Dumet, Jullian,[30] amongst others.

Yeast surface display and deep mutational scanning

Transformation of deep mutational SARS-CoV-2 RBD libraries to E. coli. Two independently generated deep mutational libraries of the SARS-CoV-2 receptor-binding domain (N331-T531) in the pETcon vector were kindly gifted by Dr. Jesse Bloom.[31] Ten ng of each plasmid pool was electroporated to *E. coli* TOP10 cells and allowed to recover for 1 h at 37 °C in SOC medium before plating on large low salt LB agar plates supplemented with ampicillin. Transformation efficiency was assessed by plating out serial dilutions. After overnight incubation, the colonies were harvested from the plates and resuspended in fresh low salt LB medium supplemented with ampicillin and grown for 2 h 30 min at 37 °C. Afterwards, the cells were pelleted, washed once with sterile MQ, and plasmid was extracted via the QIAfilter plasmid Giga prep kit (Qiagen) according to the manufacturer's instructions.

Transformation of deep mutational SARS-CoV2 RBD libraries to S. cerevisiae. Ten μg of each prepped plasmid pool were transformed to competent *S. cerevisiae* EBY100 cells according to the large-scale protocol by Gietz and Schiestl.[32] Transformed cells were selected from the transformation mixture in liquid culture by incubation in SD–trp–ura drop-out medium. After 16 h, the cultures were back-diluted at 1 OD_{600}/mL in fresh SD–trp–ura drop-out medium for an additional 9 h passage. Transformation efficiency was assessed by plating out serial dilutions. Yeast libraries were flash-frozen in 1e8 cells per aliquots and stored at –80 °C for further use.

Cloning and transformation of WT RBD of SARS-CoV-2. A double-stranded yeast codon optimized DNA fragment of the wild-type SARS-CoV2 receptor-binding domain (N331-T531) was ordered at IDT. This fragment was inserted in the pETcon vector by Gibson assembly and the resulting mixture was electroporated to *E. coli* TOP10 cells. A random selection of colonies was picked and grown for plasmid extraction via a Miniprep kit (Promega) according to the manufacturer's instructions. Correct assembly was checked via Sanger sequencing

with primers covering the RBD CDS and surrounding plasmid stretches. A sequence-verified plasmid was transformed to competent *S. cerevisiae* EBY100 cells according to the small-scale protocol by Gietz and Schiestl.[33] Transformants were identified by a yeast colony PCR with the same primers used for Sanger sequencing.

Presorting of deep mutational SARS-CoV2 RBD libraries. An aliquot of each library, as well as the control *S. cerevisiae* strain expressing SARS-CoV2 wild-type RBD, was grown in repressive SRaf–trp–ura medium for 32 h at 28 °C. Afterwards, expression was induced by back-dilution at an OD_{600} of 0.67/mL into inducing SRaf/Gal–trp–ura medium and grown for 16 h at 28 °C.

The cultures were harvested and washed thrice with FACS washing buffer (1X PBS + 1 mM EDTA, pH 7.2 + 1 Complete Inhibitor EDTA-free tablet (Roche) per 50 mL buffer). Afterwards, the cells were incubated at an OD_{600} of 8/mL in FACS staining buffer (washing buffer + 0.5 mg/mL of Bovine Serum Albumin) with 9.09 nM hACE2-muFc (Sino Biological) for 1 h. Cells were washed thrice with FACS staining buffer and incubated with 1:100 anti-cmyc-FITC (Immunology Consultants Lab), 1:1000 anti-mouse-IgG-AF568 (Molecular Probes) and 1:1000 L/D eFluor506 (Thermo Fischer Scientific) in staining buffer for 1 h. After washing thrice with staining buffer, libraries were filtered over 35 µm cell strainers and sorted on a FACSMelody (BD Biosciences), with a selection gate capturing the ACE2+ cells, such that, after compensation, max 0.1% of cells of unstained and single stained controls appeared above the background. Approximately 1 million ACE2+ cells were isolated per library in 5 mL polypropylene tubes coated with 2X YPAD + 1% BSA.

Sorted cells were recovered in liquid SD–trp–ura drop-out medium supplemented with 100 U/mL penicillin and 100 µg/mL streptomycin (Thermo Fisher Scientific) for 36 h at 28 °C, and flash-frozen in aliquots of 9 OD_{600} units.

Antibody escape mutant sorting. An aliquot of each ACE2-sorted library, as well as the control *S. cerevisiae* strain expressing SARS-CoV2 wild-type RBD, was grown in repressive SRaf–trp–ura medium for 36 h at 28 °C. Afterwards, expression was induced by back-dilution at an OD_{600} of 0.67/mL into inducing SRaf/Gal–trp–ura medium and grown for 16 h at 28 °C.

The cultures were harvested and washed thrice with FACS washing buffer (1X PBS + 1 mM EDTA, pH 7.2 + 1 Complete Inhibitor EDTA-free tablet (Roche) per 50 mL buffer). Afterwards, the cells were incubated at an OD_{600} of 8/mL in FACS staining buffer (washing buffer + 0.5 mg/mL of Bovine Serum Albumin) with 100 ng/mL tested antibody (A3, A9 or G5) for 1 h. Cells were washed thrice with FACS staining buffer and incubated with 1:100 anti-cmyc-FITC (Immunology Consultants Lab), 1:1000 anti-human-AF594 (Molecular Probes) and 1:1000 L/D eFluor506 (Thermo Fischer Scientific) in staining buffer for 1 h. After washing thrice with staining buffer, libraries were filtered over 35 µm cell strainers and sorted on a FACSMelody (BD Biosciences), with a selection gate capturing the 'escapers', chosen such that, after compensation, max. 0.1% of cells of the fully stained WT RBD control appeared in the selection gate. Approximately 78,000–-280,000 cells were captured per library in 5 mL polypropylene tubes coated with 2X YPAD + 1% BSA.

Sorted cells were recovered in liquid SD–trp–ura drop-out medium supplemented with 100 U/mL penicillin and 100 µg/mL streptomycin (Thermo Fisher Scientific) for 16 h at 28 °C before DNA extraction.

DNA extraction and Illumina sequencing. The sorted cells were subjected to plasmid extraction using the Zymoprep yeast plasmid miniprep II kit (Zymo Research) according to the manufacturer's instructions, but with the exception of a longer (2 h) incubation with the Zymolase enzyme, and with the addition of a freeze-thaw cycle in liquid nitrogen after Zymolase incubation.

A PCR with the KAPA HiFi HotStart ReadyMix using NEBNext UDI primers (20 cycles) was performed to isolate the barcode and add sample indices and remaining Illumina adaptor sequences. PCR fragments were purified once using CleanNGS magnetic beads (CleanNA), and once using AMPure magnetic beads (Beckman Coulter), and were eluted in 15 µl 0.1x TE buffer. Size distributions were assessed using the High Sensitivity NGS kit (DNF-474, Advanced Analytical) on a 12-capillary Fragment Analyzer (Advanced Analytical). Hundred bp single-end sequencing was performed on an Illumina NovaSeq 6000 by the VIB Nucleomics Core.

Analysis of sequencing data and epitope calculation. Deep sequencing reads were processed as described by Greaney, Starr[34] using the code available at https://github.com/jbloomLab/SARS-CoV-2-RBD_MAP_Crowe_antibodies, with adjustments. Briefly, nucleotide barcodes and their corresponding mutations were counted using the dms_variants package (0.8.6). The escape fraction for each barcode was defined as the fraction of reads after enrichment divided by the fraction of reads before enrichment of escape variants. The resulting variants were filtered to remove unreliably low counts and keep variants with sufficient RBD expression and ACE2 binding (based on published data: Starr, Greaney[31]). For variants with several mutations, the effects of individual mutations were estimated with global epistasis models, excluding mutations not observed in at least one single mutant variant and two variants overall. The resulting escape measurements correlated well between the duplicate experiments and the average across

libraries was thus used for further analysis. To determine the most prominent escape sites for each antibody, RBD positions were identified where the total site escape was >10 x the median across all sites and was also at least 10% of the maximum total site escape across all positions for a given antibody.

Cryogenic electron microscopy

Cryo-EM grid preparation and data collection. Purified recombinant SARS-CoV-2 S protein (6P) and the respective purified Fab fragment were mixed (12 µl total volume at a final concertation of 5.6 µM and 7.8 µM, respectively) and incubated at room temperature (RT, ~20 °C) for 10 min.

Following the incubation period, 2 µl of the mix were applied to freshly glow-discharged Quantifoil R2.1 400-mesh copper grids (EM Sciences). The grids were blotted for 3 s at RT and 95% chamber humidity and plunge-frozen in liquid ethane, at –176C, using a Cryoplunge™ 3 system (Gatan) and stored in liquid nitrogen. Cryo-EM data was acquired using a CryoARM300 (JEOL) equipped with an in-column Ω energy filter[35] and a K3 detector (Gatan) at BECM. The nominal magnification was 60,000 resulting in a calibrated pixel size of 0.76 Å/pixel. The collected movies consist of 60 frames with a total exposure time of 2.741 s and were recorded with a total dose of ~61e-/Å2 using SerialEM[36] for automated data collection at a defocus range from –1.0 to –2.4 µm.

For the complexes of SARS-COV-2 S protein bound with UZGENT_A3 or SC2/UZGENT_G5 a total of 19,584 and 8190 movies were collected, respectively.

Image processing and model building. Relion_IT as implemented in Relion-3[37] was utilized for on-the-fly data processing during the collection. The 60 frame movies were subjected to motion correction and dose weighting using MotionCor2_1.5.0.[38] Subsequently the dose-weighted aligned images were imported into Cryosparc[39] and CTF estimation was carried out using Patch CTF. A subset of the UZGENT_A3 dataset was picked with the blob picker and used for the generation of templates for subsequent picking using the template-based picker.

Particles were extracted at a box-size of 576 pixel, binned to 144 pixel and the particle sets were cleaned from junk particles by several subsequent rounds of 2D classification and selection. The cleaned particle sets were re-extracted at a box-size of 576 pixel, binned to 288 pixel, used for ab-initio reconstruction and structural heterogeneity was addressed by heterogeneous refinement using the ab-initio classes as starting models. The best classes were re-extracted un-binned and used for homogenous refinement, followed by non-uniform refinement.[40] Final resolutions, determined by gold-standard Fourier shell correlation (FSC) at 0.143, were 3.01 Å for SARS-COV-2 S protein/UZGENT_A3 and 3.02 Å for SARS-COV-2 S protein/UZGENT_G5, respectively (Fig. 8 and Supplementary Figure S5).

However, the 3D reconstructions showed significant structural variability in the region of the RBD and the bound Fab fragments making the maps difficult to interpret in these regions. To address this, masks encompassing a single RBD, the nearby NTD as well as the respective bound Fab fragment were created using USCF ChimeraX[41] and used for local refinement in Cryosparc[39] with the particle sets obtained from the final non-uniform refinement from Relion-3. The resulting refined sub-volumes had resolutions of 3.45 Å for SARS-COV-2 S protein/UZGENT_A3 and 3.76 Å for SARS-COV-2 S protein/UZGENT_G5, respectively.

The refined maps of the sub-volumes were sharpened in Phenix-1.20.1-4487[42] and the RBD, NTD and respective Fab fragment were docked into the sharpened map. Several rounds of refinement in Phenix and manual modelling in Coot-0.9.8[43] were performed until the final models were obtained. See Supplementary Table S3 for data and model statistics.

SARS-CoV-2 hamster infection model

The *in vivo* therapeutic potential of UZGENT_A3 and UZGENT_G5 as a cocktail was tested in an animal SARS-CoV-2 challenge model. KU Leuven R&D has developed and validated a SARS-CoV-2 Syrian Golden hamster infection model.[17,44] This model is suitable for the evaluation of the potential antiviral activity and selectivity of compounds/antibodies.[45] Female Syrian hamsters (*M. auratus*) were purchased from Janvier Laboratories and kept per two in individually ventilated isolator cages (IsoCage N Bio-containment System, Tecniplast) at 21 °C, 55% humidity and 12:12 day/night cycles. Housing conditions and experimental procedures were approved by the ethics committee of animal experimentation of KU Leuven (license P065-2020). For infection, female hamsters of 6–8 weeks old were anesthetized with ketamine/xylazine/atropine and inoculated intranasally with 50 µl containing 2×10^6 $TCID_{50}$ SARS-CoV-2 (day 0). On day 4 post-infection, animals were euthanized for sampling of the lungs and further analysis by i.p. injection of 500 µl Dolethal (200 mg/mL sodium pentobarbital). No randomization methods were used and confounders were not controlled, though all caretakers and technicians were blinded to group allocation in the animal facility, and to sample numbers for analysis (qPCR, titration, histology and deep sequencing). Since all animals had the same age and roughly of the same weight; all are females, we believe there is no a real confounder to be considered in the study that may impact the outcome of the experiments.

Treatment regimen. On day 0 thirty hamsters (5 treatment groups each containing 6 animals) were anesthetized with ketamine/xylazine/atropine and inoculated intranasally with 50 µl containing 2×10^6 TCID50 SARS-CoV-2 (BetaCov/Belgium/GHB-03021/2020 passage 6). One day post-inoculation with SARS-CoV-2, animals were treated once intraperitoneally. Treatments consisted of the UZGENT-COV2 antibody cocktail (=UZGENT_A3 + UZGENT_G5) 10 mg/kg or 1 mg/kg, the REGN-COV2 antibody cocktail (=REGN10933 + REGN10987) 1 mg/kg, a human IgG isotype control 10 mg/kg, or DPBS (=placebo). Hamsters were monitored daily for appearance, behavior, and weight. At day 4 post-inoculation, hamsters were euthanized by intraperitoneally injection of 500 µl Dolethal (200 mg/mL sodium pentobarbital, Vétoquinol SA) and serum and lungs were collected.

Sample size justification. For antiviral efficacy, we want to detect at least 1 $\log_{10}$ reduction in viral RNA levels in treated subjects compared to the untreated, infected control group. Group size was calculated on the independent t-test with an effect size of 2.0 and a power of 80% (effect size = deltamean/SD = 1 $\log_{10}$ decrease in viral RNA/0.5 $\log_{10}$), resulting in 5–6 animals/group. Sample sizes maximized considering limits in BSL3 housing capacity, numbers of animals that can be handled under BSL3 conditions.

Human IgG ELISA. The Human IgG ELISA kit from Abcam was used to determine the human IgG concentration in the hamsters' sera. The assay was performed according to the manufacturer's instructions using a 1:10 dilution of serum. After photometric measurement of the colour intensity made at a wavelength of 450 nm and a reference wavelength of 620 nm and generation of the standard curve, the concentration of human IgG was calculated.

SARS-CoV-2 RT-qPCR. Hamster lung tissues were collected after sacrifice and were homogenized using bead disruption (Precellys) in 350 µl RLT buffer (RNeasy Mini kit, Qiagen) and centrifuged (10,000 rpm, 5 min) to pellet the cell debris. RNA was extracted according to the manufacturer's instructions. Of 50 µl eluate, 4 µl was used as a template in RT-qPCR reactions. RT-qPCR was performed on a LightCycler96 platform (Roche) using the iTaq Universal Probes One-Step RT-qPCR kit (BioRad) with N2 primers and probes targeting the nucleocapsid.[17] Standards of SARS-CoV-2 cDNA (IDT) were used to express viral genome copies per mg tissue or per mL serum.

End-point virus titration. Lung tissues were homogenized using bead disruption (Precellys) in 350 µl MEM and centrifuged (10,000 rpm, 5 min, 4 °C) to pellet the cell debris. To quantify infectious SARS-CoV-2 particles, endpoint titrations were performed on confluent Vero E6 cells in 96-well plates.

Histology. For histological examination, the lungs were fixed overnight in 4% formaldehyde and embedded in paraffin. Tissue sections (5 µm) were analysed after staining with hematoxylin and eosin and scored blindly for lung damage by an expert pathologist. The scored parameters, to which a cumulative score of 1–9 was attributed, were the following: congestion, intra-alveolar hemorrhagic, apoptotic bodies in bronchus wall, necrotizing bronchiolitis, perivascular oedema, bronchopneumonia, perivascular inflammation, peribronchial inflammation and vasculitis.

Quantification and statistical analysis

BLI data were analysed using Octet Data Analysis (HT) software version 10.0 (ForteBio). Following the kinetics and affinity assays, data were double reference-subtracted and aligned to each other. Association and dissociation of non-saturated curves were fit in a global 1:1 model. After the epitope binning experiment, values that represent the shift in nanometres after second antibody binding to the antigen in the presence of the first antibody were normalized by subtraction of the autologous antibody control.

Following VSV-based pseudovirus neutralization assays, GFP fluorescence was normalized using the GFP fluorescence of non-infected cells and of infected cells treated with PBS. The half maximum inhibitory concentration (IC_{50}) was calculated by non-linear regression curve fitting, log(inhibitor) vs. normalized response. After SARS-CoV-2 plaque reduction neutralization tests, plaque counts were normalized using the plaque count of non-treated infected cells. The half-maximum neutralization titers ($PRNT_{50}$) were calculated by non-linear regression curve fitting, inhibitor vs. normalized response. GraphPad Prism version 9.1 was used to perform these calculations.

Succeeding the SARS-CoV-2 hamster infection experiment, viral titres in the lung tissues were calculated by the Reed and Muench method[21] using the Lindenbach calculator and were expressed as 50% tissue culture infectious dose ($TCID_{50}$) per mg tissue. Statistical differences between treatment groups were determined using the non-parametric Mann Whitney U-test. p-values of <0.05 were considered significant and statistical analyses are reported in the results and figure legends. For *in vivo* study, animals with human IgG serum level below or equal to 30% of the group-specific median value were excluded from analysis.

Role of funders

The funding source did not have any involvement in study design, data collection, data analyses, interpretation, writing of report, or decision to submit it for publication.

Results

Identification and *in vitro* characterization of two potent anti-SARS-CoV-2 antibodies

The primary goal of this study was to establish a library of neutralizing anti-SARS-CoV-2 antibodies that could be used for passive immunisation of COVID-19 patients with disabled antibody production. In the first stage, sera collected from 151 convalescent COVID-19 patients with disease severities. Samples collected from 79 mild cases as part of CoVim clinical trial (Viro-Immunological study of people infected with COVID19–NCT04904692) and 72 severe cases collected as part of CoSer clinical trial (Serological analysis of people infected with COVID–NCT0500030719) were screened for SARS-CoV-2 neutralising activity using a surrogate neutralization assay based on antibody-mediated inhibition of the SARS-CoV2-RBD interaction with ACE2 (Supplementary Table S1).[46] All serum samples were collected between March 27 and November 13 2020, when ancestral type (Wuhan) SARS-CoV-2 was the predominantly circulating strain of the virus. Based on performance of the sera in the surrogate neutralisation assay and the availability of sufficient peripheral blood mononuclear cells (PBMCs), 14 patients were selected for further investigation (Supplementary Table S2). To this end, a B cell mining platform adapted from methods described by Tiller, Meffre[23] and Robbiani, Bozzacco[24,25] was used. With a multi-colour flow cytometry panel (Supplementary Figure S1), a total of 1069 viable B-cells binding the SARS-CoV-2 RBD were sorted out, from which 398 paired heavy and light chain antibody sequences were obtained and sequenced (Supplementary Table S2) indicating approximately 35% success rate of RT-PCR and cloning process. Of note, similar workflows relying on Ab identification in B cells from convalescent patients have been widely exploited in the context of COVID-19 by both industrial and academic research groups,[25,47–63] likely because they remain one of the most straightforward strategies to extract potent Abs. An overview of the discovery pipeline is presented in Fig. 1.

Unique to our approach is that we built in an *in-silico* step, early on in the discovery pipeline, in an attempt to be able to select promising antibody candidates, binding different regions in the SARS-CoV-2 RBD, without the need for time-consuming experimental analyses. Using a combination of algorithms, the commercialized MAbSilico artificial intelligence (AI)-based method that we used[64] allows quick similarity analysis of large antibody sequence datasets, via the enumeration of common subsequences in the CDRs and without the need for structural data. Via this *in-silico* approach, a similarity matrix between the 398 antibodies was generated (Fig. 2a). Within a cluster all the antibodies are predicted to have largely overlapping epitopes.

Following cloning and small-scale recombinant production in HEK293T cells, out of the 398 cloned antibodies, 249 Abs were shown to bind the SARS-CoV-2 S1 protein by ELISA and 188 Abs could neutralize vesicular stomatitis virus-based reporter viruses pseudotyped with spike derived from Wuhan SARS-CoV-2 (Supplementary Table S2). The pipeline described here shows efficiency similar to that reported by others.[47,65] Combining evidence from the neutralization analyses with the MAbSilico cluster analysis two antibodies (CoSer3_6721A3 alias UZGENT_A3 and CoSer5_671G5 alias UZGENT_A5), belonging to different clusters (Fig. 2b), were selected for in depth MAbTope[15] antibody epitope characterization. Based on the MAbTope analyses, it was predicted that the main interaction regions of UZGENT_A3 and UZGENT_G5 largely differ (Fig. 2c), with UZGENT_G5 mainly targeting the "chest" region and UZGENT_A3 the "neck/back" region that strongly overlaps with the ACE2 binding site, according to the taxonomy proposed by Dejnirattisai, Zhou.[66]

To benchmark the UZGENT_A3 and UZGENT_G5 antibodies, in subsequent *in vitro* and *in vivo* experiments they were compared to the Abs that comprise the clinically relevant REGN-COV2 cocktail from Regeneron, REGN10933 (casirivimab) and REGN10987 (imdevimab).[67] To quantify the neutralizing capacity of the selected antibodies towards wild-type SARS-CoV-2, pseudotyped VSV that incorporates the ancestral type (Wuhan) S sequence was used. As shown in Fig. 3a, dose-response curves are close to each other and the calculated IC_{50} values of UZGENT_A3 and UZGENT_G5 proved to be very low (UZGENT_A3 2.19 ± 0.83 ng/mL; UZGENT_G5: 4.07 ± 2.93 ng/mL, n = 4). Subsequently, the *in vitro* potency of UZGENT_A3 and UZGENT_G5 to neutralize authentic SARS-CoV-2 was also assessed. Therefore, plaque reduction neutralization assays were performed with the B.1.1.7 isolate, confirming the results of the pseudovirus assay, i.e., low $PRNT_{50}$ values for both UZGENT_A3 and UZGENT_G5 antibodies (Fig. 4a and e).

To characterize *in vitro* binding of the antibodies to the SARS-CoV-2 RBD, we conducted biolayer interferometry (BLI) analysis on the Octet Red instrument using the SARS-CoV-2 RBD as ligand. Remarkably, despite similar *in vitro* and *in vivo* neutralization potencies, the affinities UZGENT_A3 and UZGENT_G5 for the RBD exceed those of the REGN antibodies with an over 40-fold higher apparent affinity for UZGENT_G5 (Fig. 5e). As evident from the binding kinetics (Fig. 5a and b), UZGENT_G5 displayed a very slow dissociation rate, which drives the low K_D. Interestingly, despite application of another technique (surface plasmon resonance), the obtained K_D for REGN10933 is very similar to the value obtained by Hansen, Baum,[53] i.e., 3.37 nM, with a SARS-CoV2 spike protein RBD ectodomain expressed with a C-terminal mycmyc-hexahistidine tag, whereas the dissociation

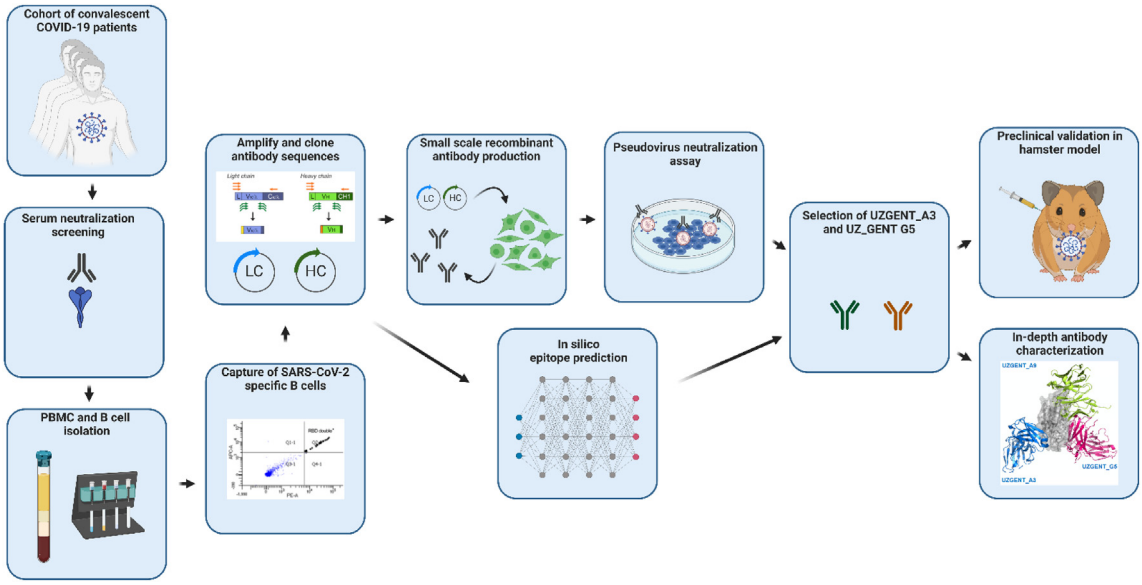

***Fig. 1:* Overview of the experimental workflow.** Sera collected from 162 convalescent COVID-19 patients were screened for the presence of neutralizing antibodies followed by RBD-specific single B cell sorting and cloning of paired heavy and light chains. Monoclonal antibodies were produced and tested for neutralization potency while *in silico* epitope binding prediction was performed in parallel, leading to selection of UZGENT_A3 and UZGENT_G5 for *in vivo* validation.

constant value acquired for REGN10987 was 10-fold higher compared to what we observed.

Preclinical *in vivo* validation of UZGENT_A3 and UZGENT_G5 in a hamster model

Next, we wanted to evaluate the *in vivo* therapeutic potential of UZGENT_A3 and UZGENT_G5 in an animal SARS-CoV-2 challenge model and preferably in a cocktail as it has been shown that Ab combinations, rather than single mAb administration, decrease the chance of escape mutants, provided that the Abs have non-overlapping epitopes.[67–72] In addition, the risk of not (completely) losing efficacy should a new variant arise is reduced and synergistic neutralizing effects have been shown *in vitro*.[62,73] As the *in silico* predictions indicated that it was rather unlikely that UZGENT_A3 and UZGENT_G5 would compete for the same residues, it was decided to test UZGENT_A3 and UZGENT_G5 as a cocktail, further designated UZGENT-COV2, in an animal model. The hamster SARS-CoV-2 infection model applied in this study has been described before (Boudewijns et al., 2020; Sanchez Felipe et al., 2020) and the specific study design is shown in Fig. 8a. Groups of 6 hamsters inoculated with SARS-CoV-2 were assigned to

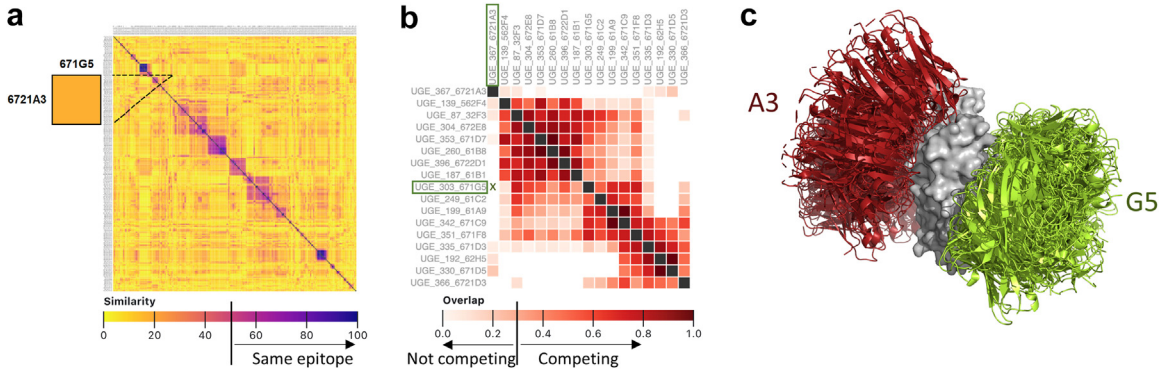

***Fig. 2: In-silico* epitope prediction.** (a) Pairwise similarity matrix between the 398 cloned antibodies. The zoom-in box is focused on the UZGENT_A3 and UZGENT_G5. (b) Prediction of most potent antibody competition for WT SARS-CoV-2 RBD binding. (c) Docking poses of UZGENT_A3 and UZGENT_G5 on WT SARS-CoV-2 RBD.

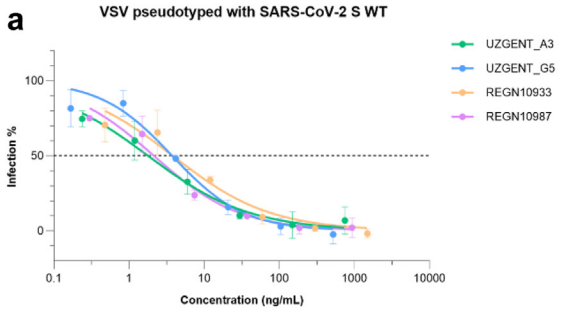

b

Antibody	WT	K417N	E484K	L452R
UZGENT_A3	1.79	0.52	> 500	1.50
UZGENT_G5	3.74	0.69	> 500	2.70
REGN10933	3.80	18.13	38.64	1.97
REGN10987	2.13	ND	ND	ND

*ND = not determined

***Fig. 3:* Potency of anti-SARS-CoV-2 spike monoclonal antibodies to neutralize pseudotyped VSV.** (a) Representative graph showing the mean ± SEM (N = 4) GFP fluorescence of VSV expressed wild-type SARS-CoV-2 S normalized to the mean GFP fluorescence of non-infected and infected PBS-treated cells. The table displays the calculated the half inhibitory concentrations (IC_{50}) in ng/mL for the WT pseudovirus and its L452R, K417N, or E484K mutants (b).

treatment with either the UZGENT-COV2 antibody cocktail at 10 mg/kg or 1 mg/kg, the REGN-COV2 antibody cocktail (=REGN10933 + REGN10987) at 1 mg/kg, a human IgG isotype control at 10 mg/kg or DPBS. It was opted to go for a therapeutic rather than prophylactic strategy as it is more challenging to control the viral load when the former is applied, as demonstrated by Cao, Su[49] and Kreye, Reincke,[74] amongst others. Three days after treatment, a significant median reduction of 4.37 log_{10} and 2.54 log_{10} in infectious virus

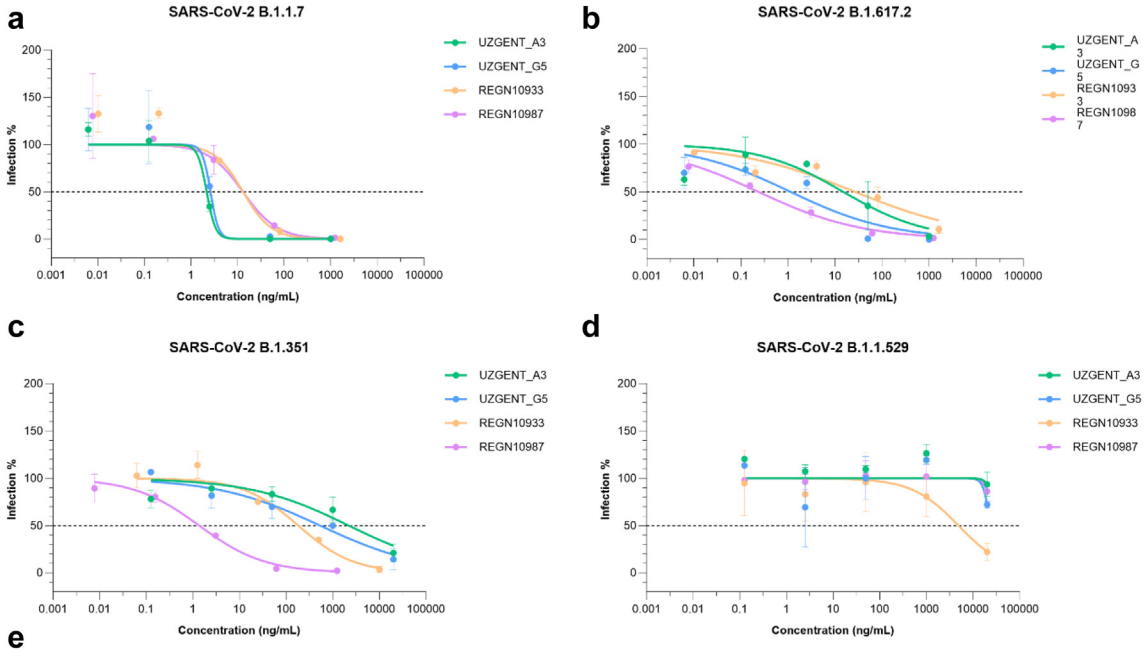

e

Antibody	B.1.1.7	B.1.351	B.1.617.2	B.1.1.529
UZGENT_A3	2.17	> 500	15.01	> 500
UZGENT_G5	2.62	> 500	1.14	> 500
REGN10933	13.15	182.30	26.55	> 500
REGN10987	13.04	1.36	0.23	> 500

***Fig. 4:* Potency of anti-SARS-CoV-2 spike monoclonal antibodies to neutralize authentic SARS-CoV-2.** Viruses that either belong to lineage B.1.1.7 (a), B.1.617.2 (b), B.1.351 (c) or B.1.1.529 (d) were used. The graphs show the mean (n = 2 ± SD) plaque counts normalized to the mean plaque count of non-treated infected cells, and the table displays the calculated the half inhibitory concentrations ($PRNT_{50}$) in ng/mL (e).

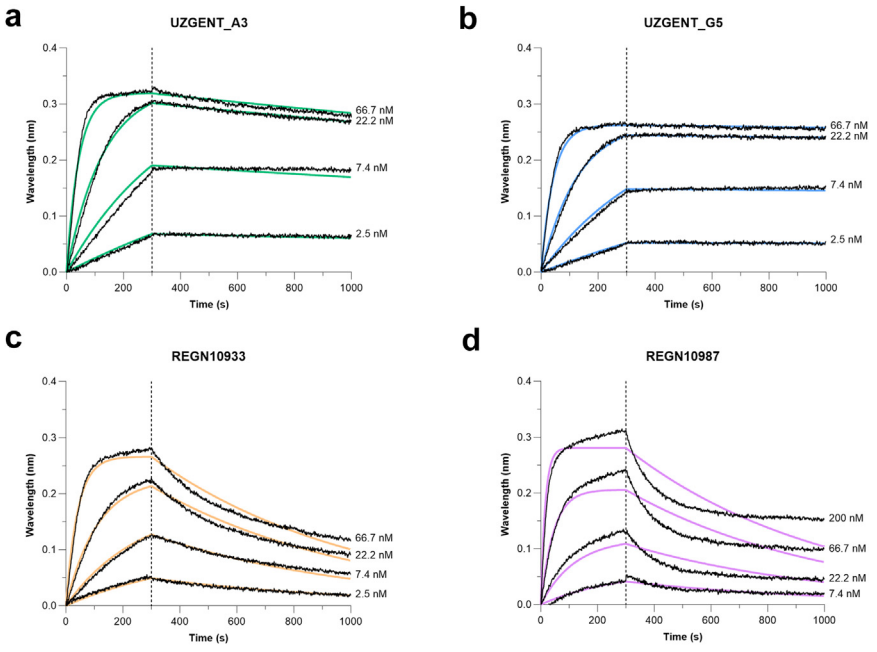

e

Antibody	K_D (M)	k_{on} (1/Ms)	k_{dis} (1/s)
UZGENT_A3	4.87E-10	3.44E+05	1.67E-04
	2.76E-10	3.74E+05	1.03E-04
	2.34E-10	4.49E+05	1.05E-04
UZGENT_G5	6.80E-11	3.52E+05	2.39E-05
	<1.0E-12	3.58E+05	<1.0E-07
	9.11E-11	4.57E+05	4.17E-05
REGN10933	3.36E-09	3.63E+05	1.22E-03
	4.03E-09	3.45E+05	1.39E-03
	3.39E-09	4.07E+05	1.38E-03
REGN10987	4.10E-09	3.18E+05	1.31E-03
	4.54E-09	3.13E+05	1.42E-03
	3.58E-09	3.60E+05	1.29E-03

f

Ab 1 \ Ab 2	UZGENT_A3	UZGENT_G5	REGN10933	REGN10987
UZGENT_A3	0	0	0.01	0.29
UZGENT_G5	0	0	0.02	0.03
REGN10933	0	-0.01	0	0.47
REGN10987	0.26	0.06	0.34	0

Fig. 5: **Kinetics, affinity, and binning assessed by bio-layer interferometry.** Kinetics and affinity assays were performed in triplicate with anti-human IgG Fc capture sensors on an Octet RED96 system (ForteBio). The sensors were loaded with antibodies and afterwards immersed in serial dilutions of purified SARS-CoV-2 RBD. Sensorgrams with binding curves (black) and global 1:1 model fits (color) of the association and dissociation phase obtained in one of the replicate experiments are shown for UZGENT_A3 (a), UZGENT_G5 (b), REGN10933 (c) and REGN10987 (d). The X-axis displays the time in seconds and the Y-axis the wavelength shift of white light interference in nanometres. The affinity constant (K_D) constants and association (k_{on}) and dissociation (k_{dis}) rates of the 3 independent measurements were also calculated using the monovalent model (e). Cross-competition between anti-SARS-CoV-2 monoclonal antibodies was evaluated using the "classical sandwich" approach. The shift in nanometres after second antibody binding to the antigen in the presence of the first antibody is shown (f). Values were normalized by the subtraction of the autologous antibody control. Conditions for which bi-directional competition was observed are marked in red, whereas in the case of self-self competition or no competition grey and yellow were used, respectively.

titre and 3.72 log_{10} and 1.33 log_{10} in viral RNA load was observed for the UZGENT-COV2 cocktail 10 mg/kg and 1 mg/kg, respectively, compared to the placebo group (Fig. 8c and d). For the commercially available REGN-COV2 cocktail, a significant median reduction of 2.77 log_{10} for viral RNA load and 3.83 log_{10} for infectious virus titer was detected, which is slightly higher compared to UZGENT-COV2 dosed at 1 mg/kg. Taken together, it was shown that UZGENT-COV2 exhibits high therapeutic efficacy *in vivo*.

Apart from viral loads, body weight was monitored daily and lungs were assessed for the presence of histopathological lesions. However, these parameters did not demonstrate extensive differences between placebo and treatment groups. This can be explained by usage of an attenuated passage 6 SARS-CoV-2 strain that encompasses tissue culture-adapted mutations and is known to have reduced fitness in WT hamsters, which translates into an absence of body weight change and attenuated pathology pattern upon infection.[17,75] Indeed, there was no statistically significant difference in histopathological lesions between treated animals and the placebo group, despite the fact that for three out of five animals treated with UZGENT-COV2 10 mg/kg a decreased lesion score was obtained (Fig. 8f), and even though a positive statistically significant effect on body weight was detected for the UZGENT-COV2 cocktail, a similar trend was also visible for the isotype control (Fig. 8e).

The presence of the human IgG antibodies in the hamsters' serum three days after administration was also assessed. Animals with outlier human IgG concentrations, most likely a consequence of an inaccuracy during antibody administration were excluded from the analysis. We observed that the human IgG serum levels for UZGENT-COV2 are much lower than expected when compared to those of the isotype control and REGN-COV-2 (Fig. 8b). This could indicate that the UZGENT Abs are cleared faster by the hamsters, which raises the question if better virus neutralization would be observed, or lower dosage regimens could be applied, if the half-life would be prolonged. This could be achieved by modifying the Fc region, which is known to play a crucial role in antibody degradation, e.g., by insertion of the LS (M428L/N434S) or YTE (M252Y/S254T/T256E) mutations that induce increased neonatal Fc receptor affinity, reduced lysosomal degradation and thus extend antibody half-life.[76–78] Alternatively, instead of being susceptible to clearance, the UZGENT Abs might present off-target binding and undergo sequestration by another binding partner.

Confronting *in silico* epitope predictions and experimental validation

Following the emergence of new SARS-CoV-2 variants of concern (VOCs) encompassing RBD mutations that abrogate the efficacy of a wide range of mAbs,[10,68,79–88] neutralization activity of the UZGENT antibodies against these variants was monitored as well. In neutralization assays with authentic SARS-CoV-2, activity against B.1.351 (beta variant) and B.1.1.529 (omicron BA.1 variant) appeared to be severely abrogated for both the UZGENT antibodies (Fig. 4c and d), whereas activity against B.1.617.2 (delta variant) was maintained (Fig. 4b). Decreased activity against B.1.351 was also observed for REGN10933, and against B.1.1.529 for both REGN Abs, which is in agreement with previously published results.[10,68,79–84,86,87] VSVs pseudotyped with SARS-CoV-2 S containing single point mutations were subsequently used to evaluate which RBD residue change(s) induce changes in efficacy for the UZGENT Abs. Pseudoviruses that encompass the K417N, E484K or L452R were included in this study since they were the hallmark mutations within the RBD of VOC (B.1.351 and B.1.617.2) circulating in Europe at the time of UZGENT antibody selection. A severely decreased neutralization of the E484K mutant (present in B.1.351) was observed for both UZGENT antibodies, whereas the L452R (present in B.1.617.2) and K471N (present in B.1.351 and B.1.1.529) mutations appeared to have little effect compared to wild type. This indicates that it is the E484K mutation that abrogates neutralization of B.1.351 by the UZGENT Abs. In B.1.1.529 the E484 residue is mutated to A instead of K; it could be assumed that the E484A mutation is responsible for the observed loss of efficacy against B.1.1.529, at least in part as other mutations within the B.1.1.529 have not been evaluated in this study. In addition, it was unexpected that residue 484 would play a crucial role in binding of UZGENT_A3 and UZGENT_G5 in view of the *in silico* epitope predictions. Indeed, the 484 residue was not designated significant, not for UZGENT_A3 nor for UZGENT_G5 (Figs. 6 and 7), although it belongs to regions that have been predicted as interaction regions in both cases. Surprisingly, residue K417 was predicted to be included in the epitope of UZGENT_A3, which has been confirmed by the EM structures (see hereafter), but mutation K417N appeared to have little impact in the neutralization assays. Of note, the results for REGN10933 are in line with observations of others,[68,84] i.e., no change in activity for the L452R mutation, but decreased neutralization of the K417N and E484K mutants.

As these (pseudo-)virus neutralization assays indicated a potential overlap in interaction region, or at least at residue 484, bio-layer interferometry was used to establish epitope binning. UZGENT_A3 and UZGENT_G5 appeared to compete with each other. Moreover, UZGENT_G5 and UZGENT_A3 both compete with REGN10933 (Fig. 5f). To verify that these observations do not stem from steric hindrance mediated by the Ab Fc portions in the BLI assay, similar experiments were performed with Fab fragments instead of full antibody, which led to the same result (data not shown). In addition, the lack of competition

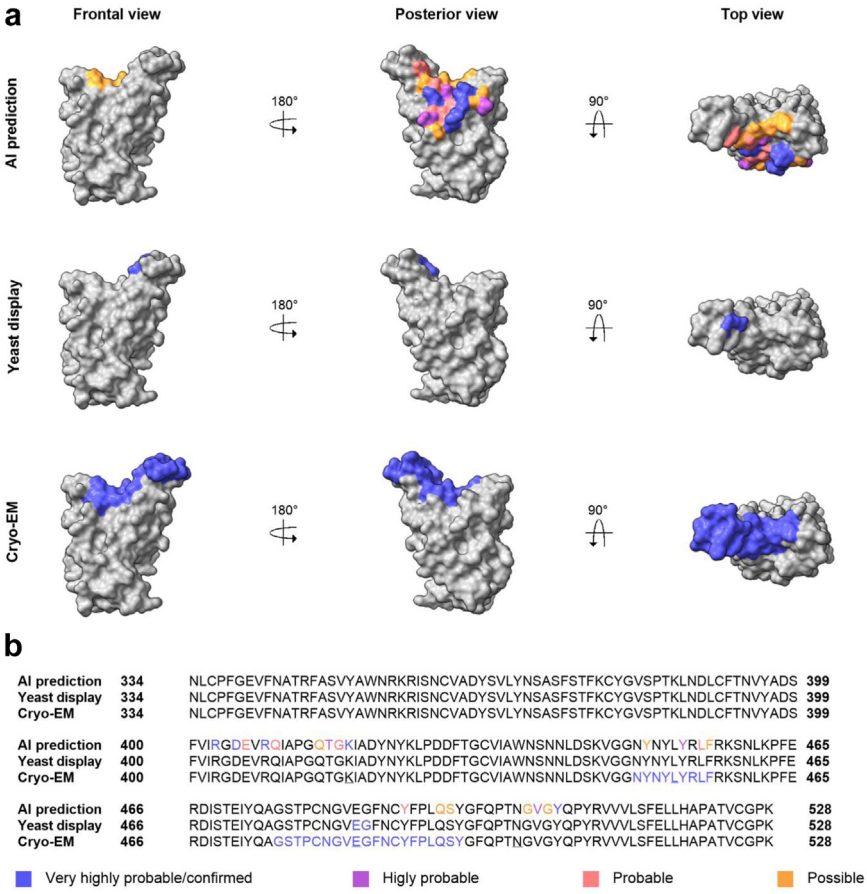

***Fig. 6:* Overview of SARS-CoV-2 RBD residues involved in UZGENT_A3 binding as determined by *in silico* and *in vitro* epitope mapping techniques.** (a) Artificial intelligence (AI)-based initial epitope predictions, and epitope residues evidenced by yeast surface display and deep mutational scanning, and cryogenic electron microscopy of UZGENT_A3 displayed on the structure of SARS-CoV-2 RBD (PDB: 6M0J[89]) (a) and sequence (b) are shown in which the (presumedly) involved residues are highlighted.

between REGN10933 and REGN10987 is conform with previous results reported by Hansen, Baum.[53]

A flow cytometry-based yeast surface display method was next applied to determine which residues within the RBD are the most crucial for interaction with UZGENT_A3 and UZGENT_G5 (Figs. 6 and 7 and Supplementary Figure S2). Residues 484 and 485 seem to be involved in binding of both UZGENT_A3 and UZGENT_G5, from which can already be concluded that they have (at least) partially overlapping epitopes. This explains the BLI binning results that were described above as well as the decreased activity against B.1.351 and pseudotyped virus containing the E484K mutation. It should be noted, however, that the actual epitope footprint would probably encompass more residues than the ones described here, in part because this assay only detects residues that strongly contribute to the interaction and can furthermore not identify residues outside the RBD nor those included in quaternary structures.

The classical procedure for epitope mapping using MAbTope is to make an initial model. MAbTope is a docking-based method, and docking poses are ranked using AI-optimized scoring functions. The four 15 residues-long regions of the target sequence containing the highest number of residues observed in the interface in the top-ranked docking poses are defined as interaction regions. Within these regions, amino acids with exposed side-chains and not participating to intramolecular interactions are suggested as mutations allowing to experimentally validate the predictions. Based on experimental binding to these mutants, a refined model can be generated. In the context of the pandemic, we wanted to be as fast as possible, and decided to trust the initial models, which indicated that UZGENT_A3 and UZGENT_G5 were probably not competing. *In vivo* experiments were started on that basis. For both antibodies, E484 and G485, which affect the binding of the antibodies, are in a region predicted

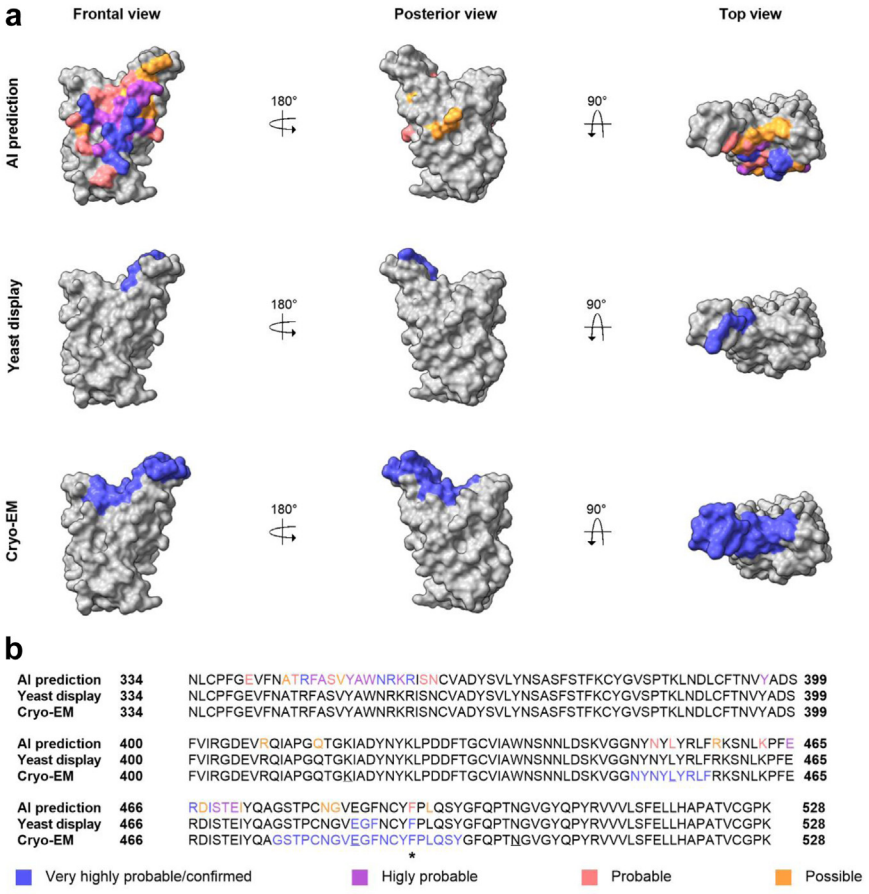

***Fig. 7*: Overview of SARS-CoV-2 RBD residues involved in UZGENT_G5 binding as determined by *in silico* and *in vitro* epitope mapping techniques.** (a) Artificial intelligence (AI)-based initial epitope predictions, and epitope residues evidenced by yeast surface display and deep mutational scanning, and cryogenic electron microscopy of UZGENT_G5 displayed on the structure of SARS-CoV-2 RBD (PDB: 6M0J[89]) (a) and sequence (b) are shown in which the (presumedly) involved residues are highlighted. Asterisks mark residues that are designated to be part of the epitope by all three techniques.

to belong to the epitope (Figs. 6b and 7b, Supplementary Figures S3 and S4).

Following Yeast display results (and before the Cryo-EM experiments), refined models were made. As shown (Supplementary Figures S3–S5), in the refined models the two antibodies are clearly competing. Moreover, for both antibodies, the two regions constituting the core of the epitopes are indeed predicted as part of the epitope.

The lower *in vivo* potency of our cocktail compared to that of Regeneron is a direct result of this competition. Infusing either UZGENT_A3 or UZGENT_G5 alone would most likely lead to the same outcome.

Final elucidation by cryo-EM

In a final attempt to experimentally resolve the paratope-epitope interactions we resorted to single particle cryo-EM. 3D reconstructions of the UZGENT_A3 and UZ_GENT G5 Fab fragments in complex with the ancestral type (Wuhan) SARS-CoV-2 S protein. Structures of these complexes were obtained at 3.35 and 3.72 Å resolution, respectively (Fig. 9 and Supplementary Figure S7; Supplementary Table S3). For both nABs, three Fab copies are found to individually bind the S protein RBDs, all residing in RBD-up position. Unexpectedly, even though the antibody paratopes and the interacting residues differ (Fig. 9; Supplementary Table S4), the overall binding pose and epitope are the same for UZGENT_A3 and UZ_GENT G5 (Fig. 9). Intriguingly, a glycosylated asparagine at position 59 appeared to contribute to the epitope/paratope interaction surface in both antibodies, even though the UZGENT_A3 and UZ_GENT G5 were isolated from different patients. Analysis with IMGT/V-QUEST software for immunoglobulin and T cell receptor V–J and V–D–J rearrangement analysis showed that the

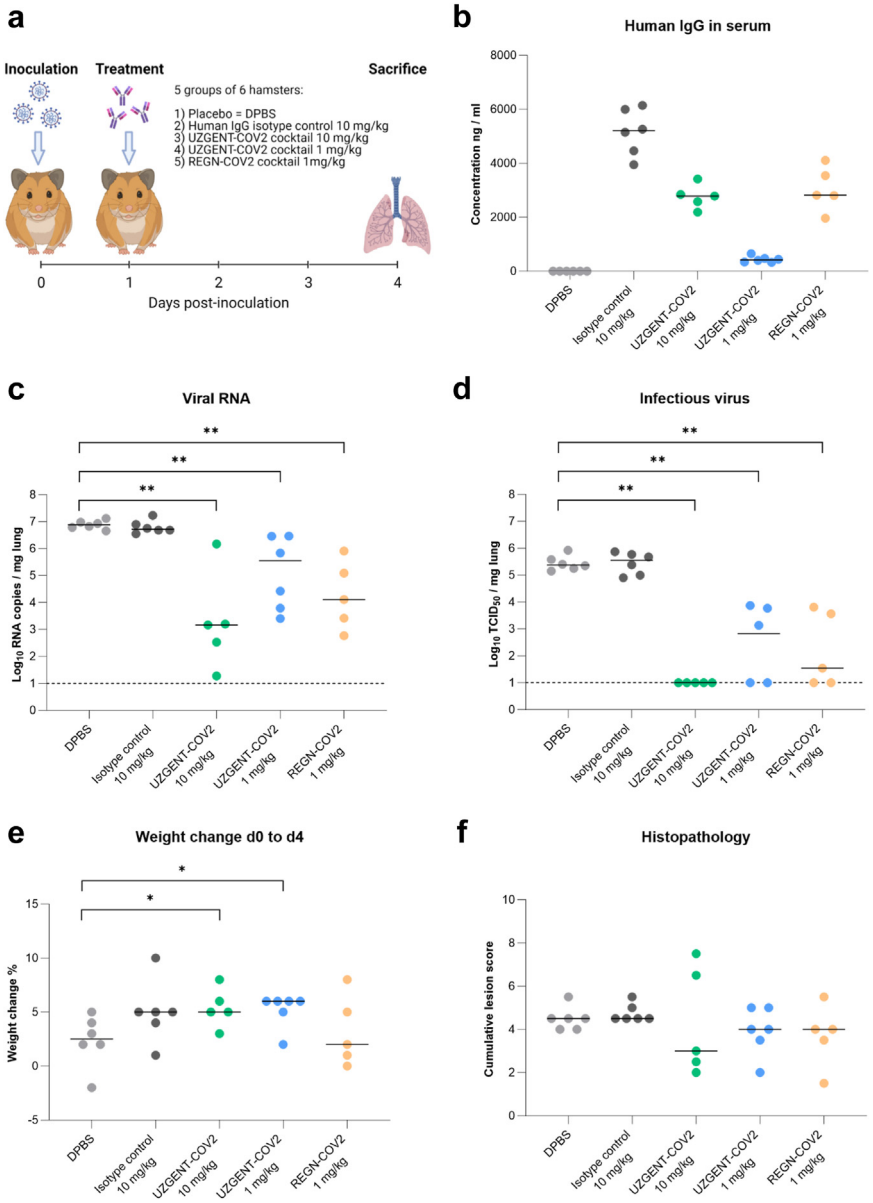

***Fig. 8:* Assessment of antibody efficacy in an animal SARS-CoV-2 challenge model.** A therapeutic strategy was applied whereby 30 hamsters were first inoculated and assigned to one of the five treatment groups 24 h later (a). Four days post-inoculation, serum was collected to determine the human IgG titers (b), and the infectious virus titer was determined by end-point virus titration (c) and viral RNA load quantified by RT-PCR (d) in the lungs of the infected hamsters. Changes in weight change were monitored from zero to four days post-inoculation (e) and cumulative lung lesion scores were obtained via histological examination (f). The median values are represented by black bars and significant differences compared to the placebo group (DPBS) were assessed by the Mann Whitney U-test and are marked with an asterisk (*$p < 0.05$; **$p < 0.01$; ***$p < 0.001$).

asparagine at position 59 is germ-line encoded within the framework region[90] and that both antibodies share the IGHV1-2*02 and IGLV2-8*01 (Supplementary Table S4). This particular V gene pair has been identified among antibodies to the SARS-CoV-2 spike protein and most frequently targets the RBD region.[91] To further elucidate the potential importance of this particular glycosylation on SARS-CoV-2 neutralization, we performed site-directed mutagenesis thereby changing the asparagine at position 59 to glutamine in the heavy chains of both the A3 and G5 antibodies. Side-by-side comparison of WT and N59Q mutants

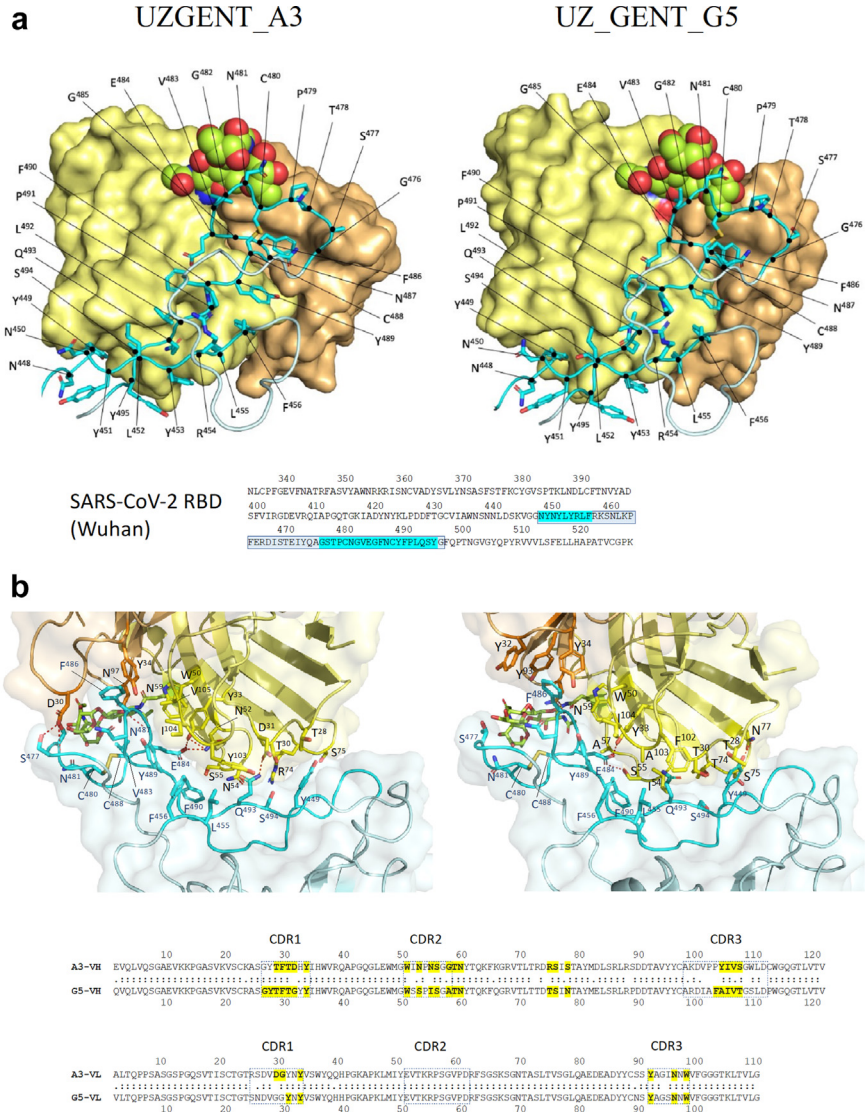

***Fig. 9:* Structures of the SARS-CoV-2 Spike with the UZGENT_A3 and UZGENT_G5 Fabs.** (a) Closeup view of the UZGENT_A3 (left) or UZGENT_G5 (right) VH (yellow) and VL (orange) domains shown in solvent accessible surface representation, in complex with the SARS-CoV-2 RBD binding epitope (cyan; residues 449–497) shown in stick representation. The N59 glycosylation is shown in sphere representation. (b) Detailed view of the Spike—Fab epitope—paratope interface, shown in stick representation (coloured as in panel a). Bottom, amino acid sequence of the UZGENT_A3 and UZGENT_G5 VH and VL domains, with residues involved in binding interactions with the RBD highlighted in yellow.

revealed that contrary to expectations, lack of glycosylation at this particular site slightly increased neutralization capacity in both cases (Supplementary Figure S6). Thus, presence of the N59 glycosylation is unlikely a strong contributing factor in the binding affinity and the remarkable convergent binding of UZGENT_A3 and UZGENT_G5 to the SARS-CoV-2 RBD with shear identical epitope and binding pose. Whether conserved glycosylation of UZGENT_A3 and UZGENT_G5 Fab's provides other beneficial properties to the antibody at the cost of neutralization remains an open question. Reports suggest that such modifications can increase their stability or promote antibody-antibody interactions.[92,93]

Discussion

Early into the SARS-CoV-2 pandemics, multiple laboratories around the world initiated research projects aimed at developing therapeutic antibodies since the prospects of fast roll-out of safe, potent and robust vaccines was uncertain. Starting from convalescent

patients B cells we used an established discovery pipeline and built in an AI-based analyses to enable rapid selection of antibodies binding different regions of the SARS-CoV-2 RBD. Although we identified two antibodies that very potently blocked the Wuhan parental viral strain, the cocktail lost effectivity against several VOCs. Experimental validation of the AI predictions demonstrated that these were inaccurate and that the selected antibodies in fact interacted with the SARS-CoV-2 RBD in a very similar manner. The 449-456 region was correctly predicted as part of the epitope for both antibodies (albeit with lowest probability score), which was validated by the Cryo-EM structures. However, in both cases this region was at the periphery of the predicted epitope, and we wrongly assumed that it was not significant, especially since the predictions with highest probability score pointed to distinct epitopes. This inaccuracy is in line with a recent review of nine state-of-the-art conformational B-cell epitope prediction webservers that achieve low performances.[94] In the original publication of the method,[15] it was shown that among the four interaction regions predicted by MAbTope for a given antibody-target pair, at least one is correct in more than 80% of tested cases. However, in about 15% of tested cases, only region 4 is correct which, unfortunately was the case for UZGENT_G5. In the case of UZGENT_A3, regions 3 and 4 were correct. As shown with MAbTope, refined predictions can be made based on experimental results obtained with mutants. In these refined predictions, 3 out of 4 regions are correct for both antibodies, and the refined prediction conclude to a competition between them. The limited accuracy of initial predictions is mostly due to the still limited number of antibody-target complexes 3D structures. Indeed, ranking of the docking poses relies on AI-based functions, which are optimized on learning sets composed of such structures. There are presently about 3000 non-redundant antibody-target complexes available, which is still low as compared to the difficulty of the task.

In retrospect, we believe that AI predictions of epitope/paratope interactions, based solely on antibody sequence information, still have important limitations. Specifically for MAbTope method used here, validation with suggested mutants and subsequent refinement of the predictions are still necessary. Including experimental medium-throughput epitope binning assays, such as BLI are instrumental for a successful antibody discovery project.

Our study is limited by the use of only one *in-silico* prediction tool. It is possible, that other algorithms and AI-based methods or their combinations would result in a different outcome. The work, however is one of the very few so far to integrate AI-based prediction in preclinical selection of therapeutic antibodies.

Contributors

D.D.A.: conceptualization, data curation and verification, formal analysis, investigation, methodology, project administration, supervision, visualization, writing—original draft. W.W.: conceptualization, data verification, funding acquisition, investigation, methodology, writing—original draft & editing. M.W.: conceptualization, investigation, methodology, writing—original draft. R.W.: investigation, methodology, writing—original draft. T.D.: funding acquisition, project administration. B.S.: conceptualization, investigation, writing—original draft. S.D.C.: conceptualization, investigation. K.S.: investigation, writing—original draft. H.E.: investigation, methodology, project administration, resources, writing—review & editing, funding acquisition. D.F.: data curation, formal analysis, methodology, project administration, resources, software, visualization, writing—review & editing. K.R.: investigation, writing—original draft. S.V.: investigation. A.P.: methodology, writing—review & editing. D.J.: supervision, writing—review & editing. X.Z.: investigation, methodology, writing—review & editing. R.A.: data curation, formal analysis, methodology, project administration, supervision, validation. C.S.F.: data curation, formal analysis, methodology, project administration, validation, writing—review & editing. B.W.: formal analysis. D.R.: investigation. N.C.: funding acquisition, methodology, supervision, writing—review & editing. H.R.: funding acquisition, supervision, validation, writing—review & editing. J.N.: funding acquisition, supervision, validation, writing—review & editing. X.S.: funding acquisition, project administration, supervision, writing—review & editing. S.G.: conceptualization, supervision, writing—review & editing. L.V.: conceptualization, funding acquisition, supervision, writing—review & editing.

All authors read and approved the final version of the manuscript.

Data sharing statement

Further information and requests for resources and reagents should be directed to and will be fulfilled by the lead contact, Linos Vandekerckhove (linos.vandekerckhove@ugent.be).

Materials availability

New antibodies were identified as part of the study, sequences of which can be found in Supplementary Table S2.

Data and code availability

- Deep mutational scanning sequencing results have been deposited at SRA and are publicly available as of the date of publication. Accession numbers are listed in the key resources table.
- Any additional information required to reanalyse the data reported in this paper is available from the lead contact upon request.
- Electron potential maps and structure coordinates for SARS-CoV-2 Spike in complex with UZGENT_A3 or UZGENT_G5 are deposited in the PDB/EMDB and PDB under accession codes 8QQ0/EMD-18571 and 8QPR/EMD-18560, respectively.

Declaration of interests

Ghent University has filed for patent protection on the antibody sequences described herein, and D.D.A., M.W., R.W., W.W., S.G. and L.V. are named as co-inventors on this patent (European Patent Application: 21186206.5). A.P. is employee of the MAbSilico, H.R. holds a patent regarding neutralizing VHH antibodies binding the Spike RBD (PCT/EP2021/052885) and has filed a priority application for neutralizing VHH antibodies binding Spike S2 (EP 23160838.1). X.S. is a recipient of FWO research project COVID-19 (G0G4920N) and FWO-FNRS project VIREOS (EOS ID: 30981113) grants.

Acknowledgements

The authors gratefully acknowledge Evelien De Smet and Ytse Noppe for their skilful technical assistance throughout the project. We thank all participants who donated samples to this study, as well as Jackeline Cecilia Zavala Marchan and Anne-Sophie De Smet for their help with

the cell cultures and the productions of viral stocks, the staff of the VIB Flow Core Ghent for providing access to flow cytometry equipment and for their technical assistance, and the staff of the VIB Nucleomics Core for Illumina sequencing.

Funding: This project was funded by Ghent University Hospital's *Fonds voor Innovatie en Klinisch Onderzoek* (FIKO) and further supported by the EOS joint programme of *Fonds de la Recherche Scientifique* (FNRS) and *Fonds Wetenschappelijk Onderzoek* (FWO) Flanders (30981113), FWO research project COVID-19 (G0G4920N), FWO-FNRS project VIREOS (EOS ID: 30981113), and UGent GOA and BOF projects of X.S. K.R. is supported by the VIB Grand Challenges Program (IBCORI, GC03-C03), H.E. by a PhD fundamental fellowship of the FWO (11C9720N), and S.D.C. by a FWO-sb fellowship (FWOSPB2020001101).

Appendix A. Supplementary data

Supplementary data related to this article can be found at https://doi.org/10.1016/j.ebiom.2023.104960.

References

1 Weinreich DM, Sivapalasingam S, Norton T, et al. REGN-COV2, a neutralizing antibody cocktail, in outpatients with Covid-19. *N Engl J Med*. 2021;384(3):238–251.
2 ACTIV-3/TICO LY-CoV555 Study Group, Lundgren JD, Grund B, et al. A neutralizing monoclonal antibody for hospitalized patients with Covid-19. *N Engl J Med*. 2021;384(10):905–914.
3 Chen P, Nirula A, Heller B, et al. SARS-CoV-2 neutralizing antibody LY-CoV555 in outpatients with Covid-19. *N Engl J Med*. 2021;384(3):229–237.
4 Gottlieb RL, Nirula A, Chen P, et al. Effect of bamlanivimab as monotherapy or in combination with etesevimab on viral load in patients with mild to moderate COVID-19: a randomized clinical trial. *JAMA*. 2021;325(7):632–644.
5 Gupta A, Gonzalez-Rojas Y, Juarez E, et al. Early treatment for Covid-19 with SARS-CoV-2 neutralizing antibody sotrovimab. *N Engl J Med*. 2021;385(21):1941–1950.
6 Kumar S, Chandele A, Sharma A. Current status of therapeutic monoclonal antibodies against SARS-CoV-2. *PLoS Pathog*. 2021;17(9):e1009885.
7 Tao K, Tzou PL, Nouhin J, et al. The biological and clinical significance of emerging SARS-CoV-2 variants. *Nat Rev Genet*. 2021;22(12):757–773.
8 Van Cleemput J, van Snippenberg W, Lambrechts L, et al. Organ-specific genome diversity of replication-competent SARS-CoV-2. *Nat Commun*. 2021;12(1):6612.
9 Zhang Y, Jiang N, Qi W, et al. SARS-CoV-2 intra-host single-nucleotide variants associated with disease severity. *Virus Evol*. 2022;8(2):veac106.
10 VanBlargan LA, Errico JM, Halfmann PJ, et al. An infectious SARS-CoV-2 B.1.1.529 Omicron virus escapes neutralization by therapeutic monoclonal antibodies. *Nat Med*. 2022;28(3):490–495.
11 Tahir S, Bourquard T, Musnier A, et al. Accurate determination of epitope for antibodies with unknown 3D structures. *MAbs*. 2021;13(1):1961349.
12 Musnier A, Bourquard T, Vallet A, et al. A new in silico antibody similarity measure both identifies large sets of epitope binders with distinct CDRs and accurately predicts off-target reactivity. *Int J Mol Sci*. 2022;23(17):9765.
13 Desta IT, Kotelnikov S, Jones G, et al. Mapping of antibody epitopes based on docking and homology modeling. *Proteins*. 2022;91(2):171–182.
14 Mahita J, Kim DG, Son S, Choi Y, Kim HS, Bailey-Kellogg C. Computational epitope binning reveals functional equivalence of sequence-divergent paratopes. *Comput Struct Biotechnol J*. 2022;20:2169–2180.
15 Bourquard T, Musnier A, Puard V, et al. MAbTope: a method for improved epitope mapping. *J Immunol*. 2018;201(10):3096–3105.
16 Lin YC, Boone M, Meuris L, et al. Genome dynamics of the human embryonic kidney 293 lineage in response to cell biology manipulations. *Nat Commun*. 2014;5:4767.
17 Boudewijns R, Thibaut HJ, Kaptein SJF, et al. STAT2 signaling restricts viral dissemination but drives severe pneumonia in SARS-CoV-2 infected hamsters. *Nat Commun*. 2020;11(1):5838.
18 Abdelnabi R, Boudewijns R, Foo CS, et al. Comparing infectivity and virulence of emerging SARS-CoV-2 variants in Syrian hamsters. *EBioMedicine*. 2021;68:103403.
19 Abdelnabi R, Foo CS, Jochmans D, et al. The oral protease inhibitor (PF-07321332) protects Syrian hamsters against infection with SARS-CoV-2 variants of concern. *Nat Commun*. 2022;13(1):719.
20 Abdelnabi R, Foo CS, Zhang X, et al. The omicron (B.1.1.529) SARS-CoV-2 variant of concern does not readily infect Syrian hamsters. *Antiviral Res*. 2022;198:105253.
21 Reed LJ, Muench H. A simple method of estimating fifty percent endpoints. *Am J Hyg*. 1938;27:493–497.
22 Wrapp D, De Vlieger D, Corbett KS, et al. Structural basis for potent neutralization of betacoronaviruses by single-domain camelid antibodies. *Cell*. 2020;181(5):1004–1015.e15.
23 Tiller T, Meffre E, Yurasov S, Tsuiji M, Nussenzweig MC, Wardemann H. Efficient generation of monoclonal antibodies from single human B cells by single cell RT-PCR and expression vector cloning. *J Immunol Methods*. 2008;329(1–2):112–124.
24 Robbiani DF, Bozzacco L, Keeffe JR, et al. Recurrent potent human neutralizing antibodies to Zika virus in Brazil and Mexico. *Cell*. 2017;169(4):597–609.e11.
25 Robbiani DF, Gaebler C, Muecksch F, et al. Convergent antibody responses to SARS-CoV-2 in convalescent individuals. *Nature*. 2020;584(7821):437–442.
26 Ogawa J, Zhu W, Tonnu N, et al. The D614G mutation in the SARS-CoV2 Spike protein increases infectivity in an ACE2 receptor dependent manner. *bioRxiv (preprint)*. 2020. https://doi.org/10.1101/2020.07.21.214932.
27 Witkowski W, Gerlo S, De Smet E, et al. Humoral and cellular responses to COVID-19 vaccination indicate the need for post-vaccination testing in frail population. *Vaccines*. 2022;10(2):260.
28 Berger Rentsch M, Zimmer G. A vesicular stomatitis virus replicon-based bioassay for the rapid and sensitive determination of multi-species type I interferon. *PLoS One*. 2011;6(10):e25858.
29 Hoffmann M, Kleine-Weber H, Schroeder S, et al. SARS-CoV-2 cell entry depends on ACE2 and TMPRSS2 and is blocked by a clinically proven protease inhibitor. *Cell*. 2020;181(2):271–280.e8.
30 Dumet C, Jullian Y, Musnier A, et al. Exploring epitope and functional diversity of anti-SARS-CoV2 antibodies using AI-based methods. *bioRxiv (preprint)*. 2020. https://doi.org/10.1101/2020.12.23.424199.
31 Starr TN, Greaney AJ, Hilton SK, et al. Deep mutational scanning of SARS-CoV-2 receptor binding domain reveals constraints on folding and ACE2 binding. *Cell*. 2020;182(5):1295–1310.e20.
32 Gietz RD, Schiestl RH. Large-scale high-efficiency yeast transformation using the LiAc/SS carrier DNA/PEG method. *Nat Protoc*. 2007;2(1):38–41.
33 Gietz RD, Schiestl RH. High-efficiency yeast transformation using the LiAc/SS carrier DNA/PEG method. *Nat Protoc*. 2007;2(1):31–34.
34 Greaney AJ, Starr TN, Gilchuk P, et al. Complete mapping of mutations to the SARS-CoV-2 spike receptor-binding domain that escape antibody recognition. *Cell Host Microbe*. 2021;29(1):44–57.e9.
35 Fislage M, Shkumatov AV, Stroobants A, Efremov RG. Assessing the JEOL CRYO ARM 300 for high-throughput automated single-particle cryo-EM in a multiuser environment. *IUCrJ*. 2020;7(Pt 4):707–718.
36 Mastronarde DN. Automated electron microscope tomography using robust prediction of specimen movements. *J Struct Biol*. 2005;152(1):36–51.
37 Zivanov J, Nakane T, Forsberg BO, et al. New tools for automated high-resolution cryo-EM structure determination in RELION-3. *Elife*. 2018;7:e42166.
38 Zheng SQ, Palovcak E, Armache JP, Verba KA, Cheng Y, Agard DA. MotionCor2: anisotropic correction of beam-induced motion for improved cryo-electron microscopy. *Nat Methods*. 2017;14(4):331–332.
39 Punjani A, Rubinstein JL, Fleet DJ, Brubaker MA. cryoSPARC: algorithms for rapid unsupervised cryo-EM structure determination. *Nat Methods*. 2017;14(3):290–296.
40 Punjani A, Zhang H, Fleet DJ. Non-uniform refinement: adaptive regularization improves single-particle cryo-EM reconstruction. *Nat Methods*. 2020;17(12):1214–1221.
41 Pettersen EF, Goddard TD, Huang CC, et al. UCSF ChimeraX: structure visualization for researchers, educators, and developers. *Protein Sci*. 2021;30(1):70–82.

42 Liebschner D, Afonine PV, Baker ML, et al. Macromolecular structure determination using X-rays, neutrons and electrons: recent developments in Phenix. *Acta Crystallogr D Struct Biol*. 2019;75(Pt 10):861–877.
43 Casanal A, Lohkamp B, Emsley P. Current developments in Coot for macromolecular model building of electron cryo-microscopy and crystallographic data. *Protein Sci*. 2020;29(4):1069–1078.
44 Sanchez-Felipe L, Vercruysse T, Sharma S, et al. A single-dose live-attenuated YF17D-vectored SARS-CoV-2 vaccine candidate. *Nature*. 2021;590(7845):320–325.
45 Kaptein SJF, Jacobs S, Langendries L, et al. Favipiravir at high doses has potent antiviral activity in SARS-CoV-2-infected hamsters, whereas hydroxychloroquine lacks activity. *Proc Natl Acad Sci U S A*. 2020;117(43):26955–26965.
46 Tan CW, Chia WN, Qin X, et al. A SARS-CoV-2 surrogate virus neutralization test based on antibody-mediated blockage of ACE2-spike protein-protein interaction. *Nat Biotechnol*. 2020;38(9):1073–1078.
47 Andreano E, Nicastri E, Paciello I, et al. Extremely potent human monoclonal antibodies from COVID-19 convalescent patients. *Cell*. 2021;184(7):1821–1835.e16.
48 Bertoglio F, Fuhner V, Ruschig M, et al. A SARS-CoV-2 neutralizing antibody selected from COVID-19 patients binds to the ACE2-RBD interface and is tolerant to most known RBD mutations. *Cell Rep*. 2021;36(4):109433.
49 Cao Y, Su B, Guo X, et al. Potent neutralizing antibodies against SARS-CoV-2 identified by high-throughput single-cell sequencing of convalescent patients' B Cells. *Cell*. 2020;182(1):73–84.e16.
50 Du S, Cao Y, Zhu Q, et al. Structurally resolved SARS-CoV-2 antibody shows high efficacy in severely infected hamsters and provides a potent cocktail pairing strategy. *Cell*. 2020;183(4):1013–1023.e13.
51 Gieselmann L, Kreer C, Ercanoglu MS, et al. Effective high-throughput isolation of fully human antibodies targeting infectious pathogens. *Nat Protoc*. 2021;16(7):3639–3671.
52 Guo Y, Huang L, Zhang G, et al. A SARS-CoV-2 neutralizing antibody with extensive spike binding coverage and modified for optimal therapeutic outcomes. *Nat Commun*. 2021;12(1):2623.
53 Hansen J, Baum A, Pascal KE, et al. Studies in humanized mice and convalescent humans yield a SARS-CoV-2 antibody cocktail. *Science*. 2020;369(6506):1010–1014.
54 Jones BE, Brown-Augsburger PL, Corbett KS, et al. The neutralizing antibody, LY-CoV555, protects against SARS-CoV-2 infection in nonhuman primates. *Sci Transl Med*. 2021;13(593):eabf1906.
55 Ju B, Zhang Q, Ge J, et al. Human neutralizing antibodies elicited by SARS-CoV-2 infection. *Nature*. 2020;584(7819):115–119.
56 Kim C, Ryu DK, Lee J, et al. A therapeutic neutralizing antibody targeting receptor binding domain of SARS-CoV-2 spike protein. *Nat Commun*. 2021;12(1):288.
57 Kreer C, Zehner M, Weber T, et al. Longitudinal isolation of potent near-germline SARS-CoV-2-neutralizing antibodies from COVID-19 patients. *Cell*. 2020;182(4):843–854.e12.
58 Shi R, Shan C, Duan X, et al. A human neutralizing antibody targets the receptor-binding site of SARS-CoV-2. *Nature*. 2020;584(7819):120–124.
59 Starr TN, Czudnochowski N, Liu Z, et al. SARS-CoV-2 RBD antibodies that maximize breadth and resistance to escape. *Nature*. 2021;597(7874):97–102.
60 Wang S, Peng Y, Wang R, et al. Characterization of neutralizing antibody with prophylactic and therapeutic efficacy against SARS-CoV-2 in rhesus monkeys. *Nat Commun*. 2020;11(1):5752.
61 Westendorf K, Zentelis S, Wang L, et al. LY-CoV1404 (bebtelovimab) potently neutralizes SARS-CoV-2 variants. *Cell Rep*. 2022;39(7):110812.
62 Zost SJ, Gilchuk P, Case JB, et al. Potently neutralizing and protective human antibodies against SARS-CoV-2. *Nature*. 2020;584(7821):443–449.
63 Zost SJ, Gilchuk P, Chen RE, et al. Rapid isolation and profiling of a diverse panel of human monoclonal antibodies targeting the SARS-CoV-2 spike protein. *Nat Med*. 2020;26(9):1422–1427.
64 Dumet C, Jullian Y, Musnier A, et al. Exploring epitope and functional diversity of anti-SARS-CoV2 antibodies using AI-based methods. *bioRxiv*. 2020. https://doi.org/10.1101/2020.12.23.424199, 2020.12.23.424199.
65 Fenwick C, Turelli P, Perez L, et al. A highly potent antibody effective against SARS-CoV-2 variants of concern. *Cell Rep*. 2021;37(2):109814.
66 Dejnirattisai W, Zhou D, Ginn HM, et al. The antigenic anatomy of SARS-CoV-2 receptor binding domain. *Cell*. 2021;184(8):2183–2200.e22.
67 Baum A, Fulton BO, Wloga E, et al. Antibody cocktail to SARS-CoV-2 spike protein prevents rapid mutational escape seen with individual antibodies. *Science*. 2020;369(6506):1014–1018.
68 Copin R, Baum A, Wloga E, et al. The monoclonal antibody combination REGEN-COV protects against SARS-CoV-2 mutational escape in preclinical and human studies. *Cell*. 2021;184(15):3949–3961.e11.
69 Dong J, Zost SJ, Greaney AJ, et al. Genetic and structural basis for SARS-CoV-2 variant neutralization by a two-antibody cocktail. *Nat Microbiol*. 2021;6(10):1233–1244.
70 Liu Z, VanBlargan LA, Bloyet LM, et al. Identification of SARS-CoV-2 spike mutations that attenuate monoclonal and serum antibody neutralization. *Cell Host Microbe*. 2021;29(3):477–488.e4.
71 Starr TN, Greaney AJ, Addetia A, et al. Prospective mapping of viral mutations that escape antibodies used to treat COVID-19. *bioRxiv [preprint]*. 2020. https://doi.org/10.1101/2020.11.30.405472.
72 Weisblum Y, Schmidt F, Zhang F, et al. Escape from neutralizing antibodies by SARS-CoV-2 spike protein variants. *Elife*. 2020;9:e61312.
73 Pinto D, Park YJ, Beltramello M, et al. Cross-neutralization of SARS-CoV-2 by a human monoclonal SARS-CoV antibody. *Nature*. 2020;583(7815):290–295.
74 Kreye J, Reincke SM, Kornau HC, et al. A therapeutic non-self-reactive SARS-CoV-2 antibody protects from lung pathology in a COVID-19 hamster model. *Cell*. 2020;183(4):1058–1069.e19.
75 Lau SY, Wang P, Mok BW, et al. Attenuated SARS-CoV-2 variants with deletions at the S1/S2 junction. *Emerg Microb Infect*. 2020;9(1):837–842.
76 Dall'Acqua WF, Kiener PA, Wu H. Properties of human IgG1s engineered for enhanced binding to the neonatal Fc receptor (FcRn). *J Biol Chem*. 2006;281(33):23514–23524.
77 Loo YM, McTamney PM, Arends RH, et al. The SARS-CoV-2 monoclonal antibody combination, AZD7442, is protective in nonhuman primates and has an extended half-life in humans. *Sci Transl Med*. 2022;14(635):eabl8124.
78 Zalevsky J, Chamberlain AK, Horton HM, et al. Enhanced antibody half-life improves in vivo activity. *Nat Biotechnol*. 2010;28(2):157–159.
79 Cao Y, Wang J, Jian F, et al. Omicron escapes the majority of existing SARS-CoV-2 neutralizing antibodies. *Nature*. 2022;602(7898):657–663.
80 Planas D, Veyer D, Baidaliuk A, et al. Reduced sensitivity of SARS-CoV-2 variant Delta to antibody neutralization. *Nature*. 2021;596(7871):276–280.
81 Planas D, Saunders N, Maes P, et al. Considerable escape of SARS-CoV-2 Omicron to antibody neutralization. *Nature*. 2022;602(7898):671–675.
82 Chen RE, Winkler ES, Case JB, et al. In vivo monoclonal antibody efficacy against SARS-CoV-2 variant strains. *Nature*. 2021;596(7870):103–108.
83 Liu L, Iketani S, Guo Y, et al. Striking antibody evasion manifested by the Omicron variant of SARS-CoV-2. *Nature*. 2022;602(7898):676–681.
84 Wang P, Nair MS, Liu L, et al. Antibody resistance of SARS-CoV-2 variants B.1.351 and B.1.1.7. *Nature*. 2021;593(7857):130–135.
85 Hoffmann M, Hofmann-Winkler H, Kruger N, et al. SARS-CoV-2 variant B.1.617 is resistant to bamlanivimab and evades antibodies induced by infection and vaccination. *Cell Rep*. 2021;36(3):109415.
86 Cameroni E, Bowen JE, Rosen LE, et al. Broadly neutralizing antibodies overcome SARS-CoV-2 Omicron antigenic shift. *Nature*. 2022;602(7898):664–670.
87 Iketani S, Liu L, Guo Y, et al. Antibody evasion properties of SARS-CoV-2 Omicron sublineages. *Nature*. 2022;604(7906):553–556.
88 Schepens B, van Schie L, Nerinckx W, et al. An affinity-enhanced, broadly neutralizing heavy chain-only antibody protects against SARS-CoV-2 infection in animal models. *Sci Transl Med*. 2021;13(621):eabi7826.
89 Lan J, Ge J, Yu J, et al. Structure of the SARS-CoV-2 spike receptor-binding domain bound to the ACE2 receptor. *Nature*. 2020;581(7807):215–220.
90 Giudicelli V, Chaume D, Lefranc MP. IMGT/V-QUEST, an integrated software program for immunoglobulin and T cell receptor V-

J and V-D-J rearrangement analysis. *Nucleic Acids Res*. 2004;32:W435–W440.
91 Wang Y, Yuan M, Lv H, Peng J, Wilson IA, Wu NC. A large-scale systematic survey reveals recurring molecular features of public antibody responses to SARS-CoV-2. *Immunity*. 2022;55(6):1105–11017.e4.
92 van de Bovenkamp FS, Derksen NIL, van Breemen MJ, et al. Variable domain N-linked glycans acquired during antigen-specific immune responses can contribute to immunoglobulin G antibody stability. *Front Immunol*. 2018;9:740.
93 Melo-Braga MN, Carvalho MB, Ferreira MCE, Felicori LF. New insights of glycosylation role on variable domain of antibody structures. *bioRxiv*. 2021. https://doi.org/10.1101/2021.04.11.439351, 2021.04.11.439351.
94 Cia G, Pucci F, Rooman M. Critical review of conformational B-cell epitope prediction methods. *Brief Bioinform*. 2023;24(1):bbac567.